Characterization of the Interactions between the Nucleoprotein and the Phosphoprotein of Henipavirus

Johnny Habchi, Stéphanie Blangy, Laurent Mamelli, Malene Ringkjøbing Jensen, Martin Blackledge, Herve Darbon, Michael Oglesbee, Yaoling Shu, Sonia Longhi

THE JOURNAL OF BIOLOGICAL CHEMISTRY VOL. 286, NO. 15, pp. 13583–13602, April 15, 2011

Characterization of the Interactions between the Nucleoprotein and the Phosphoprotein of *Henipavirus*[*] [S]

Received for publication, January 11, 2011, and in revised form, February 10, 2011 Published, JBC Papers in Press, February 11, 2011, DOI 10.1074/jbc.M111.219857

Johnny Habchi[‡], Stéphanie Blangy[‡], Laurent Mamelli[‡1], Malene Ringkjøbing Jensen[§], Martin Blackledge[§], Hervé Darbon[‡], Michael Oglesbee[¶], Yaoling Shu[¶], and Sonia Longhi[‡2]

From the [‡]Laboratoire d' Architecture et Fonction des Macromolécules Biologiques, UMR 6098 CNRS, Aix-Marseille University, Campus de Luminy, 13288 Marseille Cedex 9, France, the [§]Protein Dynamics and Flexibility by NMR Group, Institut de Biologie Structurale Jean-Pierre Ebel, UMR 5075, CEA-CNRS-UJF, 41 Rue Jules Horowitz, 38027 Grenoble, France, and the [¶]Department of Veterinary Biosciences, The Ohio State University, Columbus, Ohio 43210

The *Henipavirus* genome is encapsidated by the nucleoprotein (N) within a helical nucleocapsid that recruits the polymerase complex via the phosphoprotein (P). In a previous study, we reported that in henipaviruses, the N-terminal domain of the phosphoprotein and the C-terminal domain of the nucleoprotein (N_{TAIL}) are both intrinsically disordered. Here we show that *Henipavirus* N_{TAIL} domains are also disordered in the context of full-length nucleoproteins. We also report the cloning, purification, and characterization of the C-terminal X domains (P_{XD}) of *Henipavirus* phosphoproteins. Using isothermal titration calorimetry, we show that N_{TAIL} and P_{XD} form a 1:1 stoichiometric complex that is stable under NaCl concentrations as high as 1 M and has a K_D in the μM range. Using far-UV circular dichroism and nuclear magnetic resonance, we show that P_{XD} triggers an increase in the α-helical content of N_{TAIL}. Using fluorescence spectroscopy, we show that P_{XD} has no impact on the chemical environment of a Trp residue introduced at position 527 of the *Henipavirus* N_{TAIL} domain, thus arguing for the lack of stable contacts between the C termini of N_{TAIL} and P_{XD}. Finally, we present a tentative structural model of the N_{TAIL}-P_{XD} interaction in which a short, order-prone region of N_{TAIL} (α-MoRE; amino acids 473–493) adopts an α-helical conformation and is embedded between helices α2 and α3 of P_{XD}, leading to a relatively small interface dominated by hydrophobic contacts. The present results provide the first detailed experimental characterization of the N-P interaction in henipaviruses and designate the N_{TAIL}-P_{XD} interaction as a valuable target for rational antiviral approaches.

Hendra virus (HeV),[3] the first known member of the genus *Henipavirus* within the *Paramyxoviridae* family, emerged in 1994 as the causative agent of a sudden outbreak of acute respiratory disease in horses in Brisbane, Australia. Nipah virus (NiV), the second known member of the genus *Henipavirus*, came to light as the etiologic agent of an outbreak of respiratory and central nervous system disease in pigs and humans in Malaysia in 1998 through 1999. The initial NiV outbreak in Malaysia resulted in 265 human cases of encephalitis, including 105 deaths. The virus reemerged in Bangladesh in 2001, and outbreaks of encephalitis have occurred in that country almost every year since, with a case fatality rate approaching 75% (see (1) and references cited therein).

Although the genome of HeV and NiV shares the same overall organization of members of the *Paramyxovirinae* subfamily, a few distinctive properties, including their much larger size, led to the creation of the *Henipavirus* genus to accommodate these newly emerged zoonotic viruses (2). Currently this genus contains two virus species and a number of strains isolated from humans, bats, horses, and pigs over a wide geographic area and during a period of 10 years. Notably, henipaviruses have recently also been found outside of Australia and Asia, thus extending the number of endemic regions of one of the most pathogenic virus genera known in humans (3). The susceptibility of humans, the wide host range, and interspecies transmission, together with the absence of therapeutic agents, led to the classification of HeV and NiV as biosecurity level 4 (BSL4) pathogens (4).

As in all Mononegavirales members, the negative-strand, non-segmented RNA genome of *Henipavirus* is encapsidated by the nucleoprotein (N) within a helical nucleocapsid that has the characteristic herringbone-like structure typically observed in other *Paramyxoviridae* members (5–10). This helical nucleocapsid, rather than naked RNA, is the substrate used by the polymerase complex during both transcription and replica-

* This work was supported by the Agence Nationale de la Recherche, specific program "Physico-Chimie du Vivant", ANR-08-PCVI-0020-01, and in part by the ANR-specific program ANR-09-BLAN-0100.

[S] The on-line version of this article (available at http://www.jbc.org) contains supplemental Figs. S1–S4.

[1] Supported by a postdoctoral fellowship from the CNRS.

[2] To whom correspondence should be addressed: Architecture et Fonction des Macromolécules Biologiques, UMR 6098, 163 Avenue de Luminy, Case 932, 13288 Marseille Cedex 09, France. Tel.: 33-4-91825580; Fax: 33-491266720; E-mail: Sonia.Longhi@afmb.univ-mrs.fr.

[3] The abbreviations used are: HeV, Hendra virus; NiV, Nipah virus; N, nucleoprotein; P, phosphoprotein; L, large protein; F, fusion protein; N_{TAIL}, C-terminal disordered domain of N; IDP, intrinsically disordered protein; PMG, premolten globule; MoRE, molecular recognition element; MeV, measles virus; P_{XD}, X domain of P; SEC, size-exclusion chromatography; MALLS, multiple angle laser light scattering; RI, refraction index (refractometry); PMG, premolten globule; R_S, Stokes radius; R_S^{NF}, Stokes radius expected for a native form; R_S^{U}, Stokes radius expected for a fully unfolded form; R_S^{PMG}, Stokes radius expected for a premolten globule; MM_{theo}, theoretical molecular mass; TFE, 2,2,2-trifluoroethanol; NMR, nuclear magnetic resonance; HSQC, heteronuclear single quantum coherence; K_D, equilibrium dissociation constant; ITC, isothermal titration calorimetry; SPR, surface plasmon resonance; r.m.s.d., root mean square deviation; IMAC, immobilized metal affinity chromatography; SeV, Sendai virus; Tris, 2-[amino]-2-(hydroxymethyl)propane-1,3-diol; PDB, Protein Data Bank; RU, resonance units.

tion. Minigenome replicon studies showed that in henipaviruses the nucleoprotein, the phosphoprotein (P) and the large protein (L) proteins are necessary and sufficient to sustain replication of viral RNA (11). By analogy with other *Paramyxoviridae* members, the polymerase complex is assumed to consist of the L protein and the P protein, with this latter serving as a tether for the recruitment of L onto the nucleocapsid template. As in all Mononegavirales members, *Henipavirus* N and P proteins have been shown to interact with each other being able to form both homologous and heterologous N-P complexes (12). In addition, recent studies by Omi-Furutani *et al.* (13) allowed NiV N and P proteins to be visualized in live cells and unveiled their co-localization in the cytoplasm.

The genome organization of *Henipavirus* resembles that of the *Respirovirus* and *Morbillivirus* genera. The extra length of the *Henipavirus* genome arises mainly from additional unique, long untranslated sequences at the 3′-end of five of the six genes. Despite the much larger genome size of henipaviruses, the genome length is divisible by 6, and reverse genetics studies have confirmed that NiV obeys the "rule of six" (*i.e.* the genome length must be a multiple of 6 to replicate efficiently) (11). Overall, the proteins of henipaviruses share the same features as cognate proteins in the *Paramyxovirinae* subfamily. The *Henipavirus* P protein however is significantly larger, with a larger P N-terminal domain accounting for the extra length (14).

So far, structural and molecular information on *Henipavirus* proteins is scarce. Indeed high-resolution structural data are limited to their surface proteins, where crystallographic studies led to the determination of the three-dimensional structure of *Henipavirus* fusion (F) and attachment (G) proteins (15–18). As for the N and P proteins, the only available data come from studies carried out by Chan *et al.* (12) and from our recently published studies (14). Although Chan *et al.* (12) reported the bacterial expression of *Henipavirus* N and P proteins and performed interaction studies by protein-blotting protein-overlay assays that led to the mapping of the reciprocal N-P binding sites, those studies did not embrace any biochemical characterization of the proteins. On the other hand, in our previous studies, by combining computational and experimental approaches, we deciphered the modular organization of *Henipavirus* N and P proteins and showed that the C-terminal region of N (N_{TAIL}; amino acids 400–532) and the N-terminal region of P (amino acids 1–404/406) belong to the family of intrinsically disordered proteins (IDPs), although they both contain short, order-prone segments (14). The occurrence of some residual transient secondary and/or tertiary structure within the N_{TAIL} and the N-terminal disordered domain of P led to their classification within the premolten globules (PMG) subfamily within the family of IDPs (19–24). IDPs are ubiquitous proteins that lack highly populated secondary and tertiary structure under physiological conditions and in the absence of a partner/ligand (25) (for recent reviews on IDPs, see Ref. 26–30). IDPs exist as dynamic ensembles of interconverting conformers (31, 32).

Many IDPs have been shown to undergo a disorder-to-order transition upon binding to a partner, a phenomenon termed "induced folding" or "folding coupled to binding" (23, 33–39). IDPs recognize their partner(s) through molecular recognition elements (MoREs); these are short, order-prone regions within intrinsically disordered regions with a propensity to undergo induced folding upon binding to partners (40–43). Using bioinformatics approaches, we have previously identified, within both the HeV and NiV N_{TAIL} domains, four putative MoREs, with at least two of them (amino acids 408–422 and 473–493) exhibiting a clear α-helical nature (14). By analogy with the closely related measles virus (MeV) (44–55), we have previously speculated that the C-terminal X domain of the *Henipavirus* P protein (P_{XD}) may constitute a possible partner of *Henipavirus* N_{TAIL}, with the MoREs of this latter being involved in partner recognition (14).

In the present study, we report the bacterial expression, purification, and characterization of P_{XD} from both HeV and NiV and show that they both are structured and have a predominant α-helical content. We also show that the X domains of *Henipavirus* P proteins bind to the intrinsically disordered N_{TAIL} domain of the nucleoprotein, thereby providing a means to tether P onto the nucleocapsid template. We provide evidence for the disordered nature of N_{TAIL} domains bseng also in the context of the full-length N proteins, and show that binding to P_{XD} triggers α-helical folding of N_{TAIL}. The present studies, beyond confirming the predicted modular organization of *Henipavirus* P proteins, provide the first detailed experimental characterization of the N-P interaction and highlight the importance of disorder and induced folding in molecular recognition by *Paramyxoviridae* proteins.

EXPERIMENTAL PROCEDURES

Construction of Expression Plasmids—The *Henipavirus* N and P_{XD} constructs, encoding full-length N (residues 1–532) and residues 660–709 (NiV) or 657–707 (HeV) of P, with a hexahistidine tag fused to their C termini, were obtained by PCR using either *Pfx* (Stratagene) or Phusion (Finnzymes) polymerase and synthetic N and P genes (GenScript), optimized for the expression in *Escherichia coli*, as templates. Primers (Operon) were designed to introduce a hexahistidine tag encoding sequence at the 3′-end of the DNA fragments, as well as an *AttB1* and *AttB2* sites at the 5′- and 3′-ends, respectively. The rationale for the choice of the tag position was to avoid purification of truncated forms arising from possible abortive translation. After digestion with DpnI (New England Biolabs) to remove the methylated DNA template and purification (PCR purification kit, Qiagen), the PCR products were cloned into the pDest14 vector (Invitrogen) using the Gateway recombination system (Invitrogen).

The *Henipavirus* pDest14/N_{TAILHN} constructs encoding residues 400–532 of N with a hexahistidine tag fused to their N termini have been described (14). The NiV and HeV N_{TAIL} F527W constructs, encoding N-terminally hexahistidine tagged N_{TAIL} bearing a F527W substitution, were obtained by PCR using pDest14/N_{TAILHN} (encoding for either NiV or HeV N_{TAIL}, respectively) as template, *Turbo-Pfu* polymerase (Stratagene), and a pair of complementary mutagenic primers of 39 nucleotides in length (Operon). After digestion with DpnI to remove the methylated DNA template, the amplified PCR product was used to transform *E. coli*.

Selection and amplification of DNA constructs was carried out using $CaCl_2$-competent *E. coli* TAM1 cells (Active Motif). The sequence of the coding region of all expression plasmids was verified by sequencing (GATC Biotech) and found to conform to expectations.

Bacterial Expression and Purification of Henipavirus N, P_{XD}, and N_{TAIL} Constructs—Expression of *Henipavirus* N and N_{TAIL} constructs was carried out as described previously (14). The expression of P_{XD} constructs was carried out by growing the *E. coli* Rosetta (DE3) pLysS strain (Novagen) in 2YT medium (Triptone 16 g/liter, yeast extract 10 g/liter and NaCl 5 g/liter).

Isotopically labeled (^{15}N) N_{TAIL} samples were prepared by growing transformed Rosetta pLysS (Stratagene) cells in a 3-liter fermenter (MiniFors) at 37 °C with minimal batch medium (56) containing 100 μg/ml ampicillin and 34 μg/ml chloramphenicol and supplemented with $^{15}NH_4Cl$ (1 g/liter), and glucose (2 g/liter). A 300-ml preculture grown overnight to saturation in LB medium containing 100 μg/ml ampicillin and 34 μg/ml chloramphenicol was harvested, washed in minimal batch medium, and inoculated into the fermenter. When $A_{600\,nm}$ was between 0.8 and 1.0, protein expression was induced by the addition of 1 mM isopropyl β-D-thiogalactopyranoside, and the cells were grown overnight at 37 °C. The induced cells were harvested, washed, and collected by centrifugation (5000 × *g*, 10 min). The resulting pellets were frozen at −20 °C.

All recombinant proteins were purified using the protocol already described for *Henipavirus wt* N_{TAIL} proteins (14) with minor modifications. Briefly, cellular pellets were resuspended in 5 volumes (v/w) of buffer A (10 mM Tris/HCl, pH 7.5, 300 mM NaCl, 10 mM imidazole, and 1 mM PMSF) supplemented with 0.1 mg/ml lysozyme, 10 μg/ml DNase I, 20 mM $MgSO_4$, and protease inhibitor mixture (either one tablet (Roche Applied Science)/50 ml of bacterial lysate or 1 ml (Sigma)/25 ml of bacterial lysate depending on whether standard or isotopically labeled proteins were purified, respectively). After a 20-min incubation with gentle agitation, the cells were disrupted by sonication (using a 750W sonicator and four cycles of 30 s each at 45% power output). The lysate was clarified by centrifugation at 30,000 × *g* for 30 min. Starting from a 1-liter culture, the clarified supernatant was incubated for 1 h with gentle shaking with 2 ml of chelating Sepharose Fast Flow resin preloaded with Ni^{2+} ions (GE Healthcare) equilibrated previously in buffer A. The resin was washed with buffer A supplemented with 20 mM imidazole, and the recombinant protein was eluted in buffer A supplemented with 250 mM imidazole. Eluates were analyzed by SDS-PAGE for the presence of the desired protein product. The fractions containing the recombinant protein were combined and then loaded onto either a Superdex 200 HR 16/60 column (N and N_{TAIL} proteins; GE Healthcare) or a Superdex 75 HR 16/60 column (P_{XD} proteins). In the case of isotopically labeled N_{TAIL} samples, a protease inhibitor mixture (Sigma) was added (1 μl/ml of protein solution) prior to size-exclusion chromatography (SEC). The elution buffer for N_{TAIL} and P_{XD} proteins was either 10 mM sodium phosphate, pH 7, or 10 mM Tris/HCl, pH 7.5, in both cases supplemented with 200 mM NaCl. N proteins were eluted in 10 mM Tris buffer, pH 8, and 300 mM NaCl. Note that in the case of *Henipavirus wt* N_{TAIL} proteins, the elution from the SEC column was followed by monitoring the absorbance at 254 nm instead of 280 nm because of the lack of Trp and Tyr residues.

The proteins were concentrated using a Centricon Plus-20 (molecular cutoff of 3,000 Da for P_{XD}, 5,000 Da for N_{TAIL}, and of 10,000 Da for N) (Millipore). A protease inhibitor mixture (Sigma) was added (1 μl/ml of protein solution) to concentrated ^{15}N-labeled samples before storage. All proteins were stored at −20 °C either in the absence (N_{TAIL}) or presence of glycerol (10% for P_{XD} and 20% for N). Dialysis D-tubes (molecular cutoff of 3,500 Da) (Novagen) were used to exchange the buffer and adjust it to the ensuing analyses. All purification steps, except for gel filtrations, were carried out at 4 °C.

The apparent molecular mass of proteins eluted from preparative SEC columns was deduced from a calibration carried out with low molecular weight calibration kits (GE Healthcare). The hydrodynamic radius of a protein (Stokes radius (R_S)) can be deduced from its apparent molecular mass (as seen by SEC) (57). The theoretical Stokes radii (in Å) of a natively folded (R_S^{NF}), fully unfolded, random coil state in urea (R_S^{U}), and natively unfolded PMG (R_S^{PMG}) protein with a theoretical molecular mass (MM_{theo}) (in daltons) were calculated according to Uversky (34) as follows.

$$\log(R_S^{NF}) = 0.369*\log(MM_{theo}) - 0.254 \quad \text{(Eq. 1)}$$

$$\log(R_S^{U}) = 0.521*\log(MM_{theo}) - 0.649 \quad \text{(Eq. 2)}$$

$$\log(R_S^{PMG}) = 0.403*\log(MM_{theo}) - 0.239 \quad \text{(Eq. 3)}$$

Protein concentrations were estimated using the BCA protein assay reagent (Pierce), because estimations based on the theoretical absorption coefficients at 280 nm, as obtained using the program ProtParam at the ExPASy server, were found not to be fully reliable.

The presence of RNA in *Henipavirus* N samples was assessed as it follows. The theoretical ratio of absorptions at 260 *versus* 280 nm of a sample composed by 95% protein and 5% nucleic acid is 1.06, whereas it is 0.57 for a nucleic acid-free protein sample (58). In the nucleocapsid, because each N monomer (59 kDa) binds six ribonucleotides (330*6 = 1980 Da) (11), N represents 96% of the total nucleocapsid mass. Accordingly, the A_{260}/A_{280} ratio of N samples containing RNA is expected to be close to 1.06 (see also Ref. 5).

Analytical SEC Combined with On-line Multi-angle Laser Light Scattering and Refractometry (SEC-MALLS-RI)—Analytical SEC was carried out on a high-pressure liquid chromatography system (Alliance 2695, Waters) using silica-based columns (Shodex). A 15-ml KW-802.5 column was used for the characterization of P_{XD} and N_{TAIL} proteins as well as for monitoring complex formation between N_{TAIL} and P_{XD}. Proteins were eluted with a 10 mM Tris/HCl, pH 7.5, and 200 mM NaCl buffer at a flow of 0.5 ml/min. Separation was performed at room temperature. Typically, 30 μl of a protein solution in the 0.3–1.5 mM concentration range was injected. Detection was performed using a triple-angle light-scattering detector (MiniDAWN™ TREOS, Wyatt Technology), a quasi-elastic light-scattering instrument (Dynapro™, Wyatt Technology), and a differential refractometer (Optilab® rEX, Wyatt Technol-

ogy). Molecular mass and R_S determinations were performed by the ASTRA V software (Wyatt Technology) using a *dn*/*dc* value of 0.185 ml/g. The column was calibrated with proteins of known Stokes radii and molecular masses.

Limited Proteolysis of Henipavirus N—Proteolysis of purified N proteins (each at 16 μM) was performed in 10 mM Tris/HCl buffer, pH 8, at room temperature with trypsin (Promega Corp.). The final enzyme:substrate molar ratio was 1:400. The extent of proteolysis was evaluated by SDS-PAGE analysis of 10-μl aliquots that were removed from the reaction mixture over a time course (0, 2, 5, 10, 20, and 60 min), added to 10 μl of 2× Laemmli sample buffer, and boiled for 5 min to inactivate the protease.

Mass Spectrometry (MALDI-TOF)—Mass analysis of all *Henipavirus* proteins was performed using an Autoflex II TOF/TOF. Spectra were acquired in the linear mode. Samples (0.7 μl containing 15 pmol) were mixed with an equal volume of sinapinic acid matrix solution, spotted on the target, and then dried at room temperature for 10 min. The mass standard was either myoglobin or BSA depending on whether N_{TAIL} and P_{XD} or N proteins were analyzed, respectively. Proteins were analyzed in the Autoflex matrix-assisted laser desorption ionization/time of flight (MALDI-TOF; Bruker Daltonics, Bremen, Germany).

The identity of all purified *Henipavirus* proteins was confirmed by mass spectral analysis of tryptic fragments. The latter was obtained by digesting (with 0.25 μg of trypsin) 1 μg of purified recombinant protein obtained after separation onto SDS-PAGE. The tryptic peptides were analyzed as described above, and peptide fingerprints were obtained and compared with an *in silico* protein digest (Biotools, Bruker Daltonics). The mass standards were either autolytic tryptic peptides or peptide standards (Bruker Daltonics).

Circular Dichroism (CD)—CD spectra were recorded at 20 °C on a Jasco 810 dichrograph equipped with a Peltier thermoregulation system, using either 1-mm (N_{TAIL} F527W variants) or 0.01-mm (*wt* N_{TAIL}, P_{XD} and *wt* N_{TAIL} + P_{XD} mixtures) thick quartz cells. The buffer was either 10 mM sodium phosphate, pH 7, for N_{TAIL} F527W, or 10 mM Tris/HCl, pH 7.5, and NaCl 200 mM for *wt* N_{TAIL}, P_{XD}, and *wt* N_{TAIL} + P_{XD} mixtures. CD spectra were measured between 190 and 260 nm with a scanning speed of 20 nm/min and a data pitch of 0.2 nm. Spectra were averaged from three scans. Moreover, for each protein sample, at least three independent acquisitions were carried out so as to estimate the experimental error arising from sample preparation. The contribution of buffer was subtracted from experimental spectra. Spectra were smoothed using the "means-movement" smoothing procedure implemented in the SpectraManager package. Structural variations were measured as a function of changes in the initial CD spectrum upon addition of either 20% 2,2,2-trifluoroethanol (TFE) (Fluka) to N_{TAIL} F527W proteins or of molar excesses of P_{XD} or lysozyme (Sigma) to *wt* N_{TAIL} proteins.

Mean ellipticity values per residue ([Θ]) were calculated as $[\Theta] = 3300\, m\, \Delta A/(lcn)$, with l (path length) in cm, n = number of residues, m = molecular mass in daltons, and c = protein concentration expressed in mg/ml. The number of residues (n) is 140 for all N_{TAIL} proteins, 58 for HeV P_{XD}, 57 for NiV P_{XD}, and 129 for lysozyme, and m values are 15,241 Da for HeV N_{TAIL}, 14,949 Da for NiV N_{TAIL}, 15,280 Da for HeV N_{TAIL} F527W, 14,988 Da for NiV N_{TAIL} F527W, 6,871 Da for HeV P_{XD}, 6,733 Da for NiV P_{XD}, and 14,300 Da for lysozyme. Protein concentrations of 0.1 mg/ml were used when recording the spectra of N_{TAIL} F527W proteins either in the presence or absence of 20% TFE. Protein concentrations of 10 mg/ml were used when recording the CD spectra of either individual *wt* N_{TAIL} and P_{XD} proteins or protein mixtures (*i.e.* N_{TAIL} + P_{XD} and N_{TAIL} + lysozyme). In the case of protein mixtures, mean ellipticity values per residue ([Θ]) were calculated as $[\Theta] = 3300\, \Delta A/\{[(c_1 n_1)/m_1) + (c_2 n_2/m_2)]l\}$, where l (path length) = 0.001 cm, n_1 or n_2 = number of residues, m_1 or m_2 = molecular mass in daltons, and c_1 or c_2 = protein concentration expressed in mg/ml for each of the two proteins in the mixture. The theoretical average ellipticity values per residue ($[\Theta]_{avg}$), assuming that neither unstructured-to-structured transitions nor secondary structure rearrangements occur, were calculated as follows: $[\Theta]_{Ave} = [([\Theta]_1 n_1) + ([\Theta]_2 n_2 R)]/(n_1 + n_2 R)$, where $[\Theta]_1$ and $[\Theta]_2$ correspond to the measured mean ellipticity values per residue, n_1 and n_2 to the number of residues of each of the two proteins, and R to the excess molar ratio of protein 2.

The experimental data in the 190 to 260-nm range were analyzed using DICHROWEB (supported by grants to the Biotechnology and Biological Sciences Research Council (BBSRC) Centre for Protein and Membrane Structure and Dynamics (59, 60)). The CDSSTR deconvolution method was used to estimate the content in α-helical and disordered structure using the reference protein set 7. Reconstructed curves superimposed very well on the experimental ones, thus attesting the reliability of the inferred α-helical percentages (data not shown).

Two-dimensional NMR—P_{XD} samples at 80 μM (NiV) or 575 μM (HeV) in 10 mM sodium phosphate, pH 7, 150 mM NaCl, and 10% D_2O were used for the acquisition of bidimensional nuclear Overhauser enhancement (2D-NOESY) spectra on either a 600-MHz ultra-shielded-plus Avance-III Bruker spectrometer equipped with a TCI cryoprobe or a 500-MHz ultra-shielded-plus Avance-III Bruker spectrometer equipped with a QXI probe, respectively. The temperature was set to 300 K, and the spectra were recorded with 2048 complex points in the directly acquired dimension and 512 points in the indirectly detected dimension.

Two-dimensional heteronuclear single quantum coherence (HSQC) spectra of both HeV and NiV *wt* N_{TAIL} proteins, either alone or after the addition of various amounts of the corresponding unlabeled P_{XD} protein, were recorded at 283 K on an ultra-shielded-plus Avance-III Bruker spectrometer equipped with a cryoprobe operating at a ^1H resonance frequency of 600 MHz. All labeled N_{TAIL} samples were dissolved in 50 mM sodium phosphate, pH 7, containing 150 mM NaCl. The unlabeled P_{XD} samples were dissolved in the same buffer supplemented with 10% glycerol. The spectra were recorded with 1024 complex points in the directly acquired dimension and 64 points in the indirectly detected dimension. These NMR titration experiments were carried out first by recording the ^1H-^{15}N HSQC spectra of ^{15}N-N_{TAIL} proteins alone and then by successively recording the spectra of mixtures resulting from the addition of increasing amounts of the unlabeled protein. For the NiV N_{TAIL}-P_{XD} couple, the N_{TAIL}:P_{XD} molar ratios used were:

1:0.219, 1:0.438, 1:0.657, 1:0.876, 1:1.316, 1:1.754, and 1:2.63. For the HeV N_{TAIL}-P_{XD} couple, the N_{TAIL}:P_{XD} molar ratios used were: 1:0.97, 1:1.56, 1:2.14, 1:3.89, 1:8.55, and 1:13.24. In the course of titration, the concentration of the labeled sample dropped from 135 to 84 μM in the case of NiV ^{15}N-N_{TAIL} and from 53 to 31 μM in the case of HeV ^{15}N-N_{TAIL}. The number of scans was adjusted to take into account this gradual dilution.

Solvent suppression was achieved by using excitation sculpting with gradients (61). The data were processed using NMRPipe (62) and analyzed using the CCPN software (63).

Quantitative analysis of NMR titration data was performed as described by Bernard *et al.* (53). The dissociation constant (K_D) can be estimated from the changes in chemical shifts of the ^{15}N-labeled protein (P) caused by the addition of the unlabeled binding partner (L), by fitting the chemical shift changes to the following equation for a two-state model in fast exchange,

$$\Delta\delta_{ppm} = \frac{\Delta\delta_{max}}{2[L]}\left([P] + [L] + K_D - \sqrt{([P] + [L] + K_D)^2 - 4[P][L]}\right) \quad \text{(Eq. 4)}$$

where $\Delta\delta_{ppm}$ is the combined chemical shift variation, $\Delta\delta_{max}$ is the maximum chemical shift deviation between the free and the bound state of protein (P), and [*P*] and [*L*] are the total protein and ligand concentrations, respectively. Curve fitting over experimental data was performed by using the XCRVFIT program (R. Boyko and B. D. Sykes, University of Alberta, Edmonton, Alberta, Canada).

Fluorescence Spectroscopy—Fluorescence spectra of the single tryptophan in both the HeV and NiV N_{TAIL} F527W variants were recorded by using a Cary Eclipse (Varian) equipped with a front face fluorescence accessory at 20 °C, with 5 nm excitation and 5 nm emission bandwidths. The excitation wavelength was 290 nm, and the emission spectra were recorded between 300 and 450 nm. Titrations were performed in a 1-ml quartz fluorescence cuvette containing 1 μM N_{TAIL} F527W in 10 mM Tris/HCl, pH 7.5, 200 mM NaCl and by gradually increasing the P_{XD} concentration from 1 to 60 μM. Experimental fluorescence intensities were corrected by subtracting the spectrum obtained with the corresponding P_{XD} protein (note that P_{XD} is devoid of tryptophan residues). Data were analyzed by plotting either the relative fluorescence intensities at the maximum of emission or the wavelength at the maximum emission as a function of increasing P_{XD} concentrations.

Isothermal Titration Calorimetry (ITC)—ITC experiments were carried out on an ITC200 isothermal titration calorimeter (Microcal, Northampton, MA) at 20 °C. In these studies, the concentration of N_{TAIL} proteins was initially adjusted to 150–200 μM in the microcalorimeter cell (0.2 ml). The corresponding P_{XD} protein (stock solution at 1.5–2.2 mM) was added from a computer-controlled 40-μl microsyringe via a total of 19 injections of 2 μl each at intervals of 180 s. Whatever the binding reaction being studied, the pair of proteins used in each binding assay was dialyzed against a 10 mM Tris/HCl, pH 7.5, buffer, supplemented with either 0.2 or 1 M NaCl to minimize undesirable buffer-related effects. The dialysis buffer was used in all preliminary equilibration and washing steps. For each binding reaction, a control experiment was carried out by injecting the ligand in a cell containing only the buffer. In that way, possible heat dilution effects of the ligand could be taken into account. A theoretical titration curve was fitted to the experimental data using Origin software (Microcal). This software uses the relationship between the heat generated by each injection and ΔH° (enthalpy change in cal mol^{-1}), K_A (association binding constant in M^{-1}), n (number of binding sites/monomer), total protein concentration, and free and total ligand concentrations. The variation in the entropy (ΔS in cal mol^{-1} deg^{-1}) of each binding reaction was inferred from the variation in the free energy (ΔG), where this latter was calculated from the following relationship: $\Delta G = -RT\ln 1/K_A$.

Surface Plasmon Resonance (SPR) Studies—Binding between purified NiV N_{TAIL} and NiV P_{XD} proteins was analyzed by using BIAcore 3000 (Amersham Biosciences). Purified NiV P_{XD} (1.4 μg/ml in acetate buffer, pH 5.5) was covalently bound to carboxy-methyl groups of CM5 sensor chips using amine-coupling chemistry (Amersham Biosciences). The levels of immobilized NiV P_{XD} were between 45 and 67 RU (1000 RU equal a change in mass of 1 ng/mm^2 on the sensor surface). Kinetic and equilibrium constants were calculated from global kinetic and steady state analyses of reactions using a range of NiV N_{TAIL} analyte concentrations (*i.e.* 0.1, 0.2, 0.5, 1, 2, 5, 10, 20, and 50 μM) in HBS-P buffer (10 mM Hepes, pH 7.4, 150 mM NaCl, and 0.005% surfactant P-20). Reactions were performed at 25 °C. Sensorgrams plotted changes in surface plasmon resonance (measured in RU) as a function of time. Multiple sensorgrams representing various analyte concentrations were analyzed by using the BIAevaluation 3.1 software. Background interaction of the NiV N_{TAIL} analyte with the sensor surfaces was measured on flow channels that were activated and subsequently blocked under buffer conditions used to immobilize P_{XD}. This background was subtracted from all binding curves prior to the analyses. Immobilized lactoferrin was used as a specificity control, and the resultant sensorgrams ruled out high affinity interactions between NiV N_{TAIL} and this irrelevant protein ligand (data not shown).

For the kinetic analysis, global fitting of experimental data to well characterized binding reactions was used to define the reaction rate and equilibrium constants. Curves generated with serial analyte concentrations were applied globally to the 1:1 Langmuir binding model with or without correction for baseline drifting depending on base-line status. For steady state analysis, the equilibrium response (R_{eq}) as a function of mobile analyte concentration ([*A*]) was fit to the equation expected for a simple 1:1 Langmuir binding model using non-linear least squares (64, 65).

$$R_{eq} = R_{max}/(1 + K_D/[A]) \quad \text{(Eq. 5)}$$

In the expression above, R_{max} is the SPR response when binding is saturated, and K_D is the equilibrium dissociation constant governing the binding reaction.

For both kinetic and equilibrium analyses, the χ^2 value and residual values were used to evaluate the quality of fit between experimental data and individual binding models. Plots of residuals indicate the difference between the experimental and reference data for each point in the fit. The χ^2 value represents

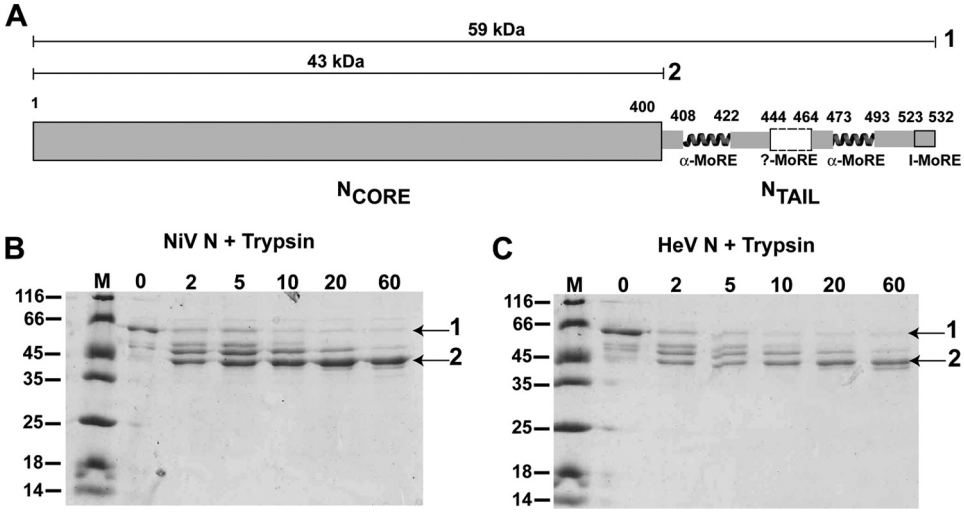

FIGURE 1. *A*, modular organization of *Henipavirus* N proteins according to Habchi *et al*. (14). The *large* and *narrow boxes* correspond to the predicted structured and disordered regions, respectively. The predicted MoREs within N_{TAIL} are also shown. *B* and *C*, 15% SDS-PAGE analysis of a time course trypsin digestion of NiV (*B*) and HeV (*C*) nucleoproteins. The extent of digestion of the purified N proteins at different time intervals (0, 2, 5, 10, 20, and 60 min) is shown. *Arrows 1* and *2* highlight undigested N (59 kDa) and a 43-kDa resistant fragment, respectively. *M*, molecular mass markers. *Numbers 1* and *2* in *panel A* correspond to bands highlighted by *arrows 1* and *2* in *panels B* and *C*.

the sum of squared differences between the experimental data and reference data at each point. A good fit between experimental and reference data has small residuals in the −2 to +2 range that randomly distribute about the *x* axis and χ^2 values that are less than 10.

Bioinformatics Analyses—Sequences for this study were obtained from the VaZyMolO database (66). Sequence accession numbers for P_{XD} are VaZy83 (HeV), VaZy2 (NiV), and VaZy91 (MeV). Sequence accession numbers for N_{TAIL} are VaZy82 (HeV), VaZy1 (NiV), and VaZy90 (MeV). Sequence similarity and identity were calculated using the EMBOSS program. Multiple sequence alignments were obtained using ClustalW (67) and drawn using ESPript (68). Secondary structure predictions were carried out using the PSIPRED server (69).

Structural Modeling—Henipavirus P_{XD} models were generated using the SAM-06 server that uses iterative hidden Markov model-based methods for constructing protein family profiles, using only sequence information (70–72). SAM-06 is a fully automated server that generates a three-dimensional structural model by making use of a set of (distantly) related homologous structures.

For both HeV and NiV, the α-helical models of the N_{TAIL} region, predicted to adopt an α-helical conformation within the putative α-MoRE encompassing residues 473–493 (see Fig. 1*A* and Ref. 14), were obtained using Swiss PdbViewer (73). This software was also used to generate the models of the NiV and HeV complexes consisting of P_{XD} and of the above mentioned α-helix of N_{TAIL}. This latter helix was modeled at the P_{XD} surface by using the crystal structure of a measles virus chimeric construct encompassing P_{XD} and residues 486–504 of N_{TAIL} (PDB code 1T6O) (74) as the template for structural alignment and the "explore fragment alternate fits" function of Swiss PdbViewer. Energy minimization of the models was carried out using the GROMOS96 implementation (75) of Swiss PdbViewer. Twenty steps of steepest descent energy minimization were performed. Models were further refined manually to avoid steric clashes using the idealization restraint of Coot (76). The quality of the final models was evaluated using MolProbity (77).

The Protein Interfaces, Surfaces, and Assemblies (PISA) server (78) was used to analyze the interface in the models of both complexes. The server PDBeFold from EMBL-EBI was used to compute root mean square deviations (r.m.s.d.) between the models and the template. The molecular graphics software PyMOL was used to visualize and draw the models (79).

RESULTS

Purification of Henipavirus N Proteins and Assessment of the Disordered State of Their N_{TAIL} Domains—We recently showed that the nucleoproteins of henipaviruses consist of an N-terminal region predicted to be structured (N_{CORE}; amino acids 1–399) and a C-terminal region (N_{TAIL}; amino acids 400–532) that is mostly disordered in solution, although it contains some residual transient secondary structure (see Fig. 1*A*) (14). As a first step in view of assessing whether these N_{TAIL} domains are also disordered in the context of the full-length nucleoproteins, we have cloned both NiV and HeV N genes (with a hexahistidine tag-encoding fragment) into the pDest14 expression plasmid, which allows expression in *E. coli* of recombinant proteins under the control of the T7 promoter.

Both HeV and NiV N proteins were recovered from the soluble fraction of bacterial lysates and purified to homogeneity (>95%) in two steps: immobilized metal affinity chromatography (IMAC) and preparative SEC (data not shown). The final purified proteins migrate in SDS-PAGE with an apparent molecular mass close to the value expected from their primary structure (~59 kDa) (see Fig. 1, *B* and *C*, *lanes 0*). The identity of the final purified proteins was confirmed by mass spectrometry analysis of the tryptic fragments obtained after digestion of the purified proteins excised from SDS-polyacrylamide gels (data not shown). Both purified N proteins were found to be partially

degraded in their C-terminal moieties (see Fig. 1, *B* and *C*, *lanes 0*), as judged from mass spectrometry (data not shown). Both nucleoproteins were eluted in the dead volume of the preparative SEC column (not shown). This indicates a molecular mass greater than 1300 kDa, which could correspond either to unspecific aggregates or to high degree multimers of N. Because N proteins from *Paramyxoviridae* members, including MeV (5) and NiV (80), are well known to form nucleocapsid-like particles when expressed in heterologous hosts, we examined the ratio between the absorbance of purified nucleoproteins at 280 and at 260 nm which gives indications on their RNA content. The A_{260}/A_{280} ratio for N devoid of RNA is 0.57, whereas it is ≥1.06 for the N-RNA complex containing six ribonucleotides/N monomer (see "Experimental Procedures"). The ratios measured for the HeV and NiV purified recombinant N proteins are 1.35 and 1.17, respectively, suggesting the presence of RNA within these nucleoproteins.

We next investigated both N proteins by limited proteolysis. We had shown previously that both isolated N_{TAIL} domains are highly susceptible to proteolysis (14). Herein we used limited proteolysis to assess whether the N_{TAIL} domains were similarly sensitive to proteolysis in the context of the full-length proteins. To establish the proteolytic pattern of the HeV and NiV nucleoproteins, we incubated them in the presence of trypsin for increasingly longer periods up to 60 min (see Fig. 1, *B* and *C*). After only 2 min of incubation, both N proteins began to be degraded, giving rise to three discrete protein fragments also detectable as minor bands in the undigested N samples (see Fig. 1, *B* and *C*). Upon increasing incubation times, a resistant fragment of ~43 kDa was obtained (see Fig. 1, *B* and *C*, *lanes 60* and *arrows 2*). Mass spectrometry analysis of this fragment showed that, for both NiV and HeV, it is composed of the N-terminal moiety of N (data not shown). On the other hand, no fragment corresponding to the remaining N_{TAIL} domain was detected, indicating that it is hypersensitive to proteolysis and entirely degraded in the context of the entire N proteins either.

Purification and Characterization of Henipavirus P_{XD}—We recently deciphered the modular organization of *Henipavirus* phosphoproteins using bioinformatics approaches and showed that they both contain a C-terminal X domain (referred to as P_{XD}) predicted to be folded and to adopt an α-helical conformation (see Fig. 2*A* and supplemental Fig. S1*A*) (14). To assess the ability of *Henipavirus* P_{XD} to interact with the disordered N_{TAIL} domains of the N proteins, we cloned the P_{XD}-encoding P gene fragments into the pDest14 expression plasmid and expressed them as a fusion with a C-terminal hexahistidine tag.

Both NiV and HeV P_{XD} were found to be soluble in *E. coli* and were purified to homogeneity (>95%) in two steps: IMAC and preparative SEC (data not shown). The final purified proteins migrate in SDS-PAGE with an apparent molecular mass close to the value expected from their primary structure (~6.6 kDa) (see Fig. 2*B* and supplemental Fig. S1*B*). The identity of the final purified proteins was confirmed by mass spectrometry analysis of the tryptic fragments obtained after digestion of the purified proteins excised from SDS-polyacrylamide gels (data not shown). The molecular masses measured by MALDI-TOF for NiV P_{XD} (6740 ± 3 Da) and for HeV P_{XD} (6737 ± 3 Da) are consistent with the values expected for full-length proteins in which the initial methionine is either conserved (NiV) or cleaved off (HeV). These findings are in agreement with previous studies showing that in proteins expressed in *E. coli* the initial methionine is generally cleaved off when followed by small residues such as glycine or alanine (81).

The oligomeric state of both P_{XD} proteins was investigated by using analytical SEC-MALLS-RI. HeV P_{XD} was found to be monomeric even when loaded onto the SEC column at concentrations as high as 1.1 mM. Under these conditions, its observed molecular mass is 7222 ± 620 Da (see Fig. 2C) and its measured R_S is 13.1 ± 1.9 Å, in agreement with the theoretical value (14.4 Å) expected for a folded protein (57). Furthermore, the sharpness and symmetry of the obtained peak indicates the presence of a well defined molecular species, demonstrating the homogeneity (*e.g.* monodispersity) of the sample. Conversely, NiV P_{XD} was found to be trimeric even at concentrations as low as 0.3 mM and up to 1.1 mM, a condition in which the estimated molecular mass is 19,820 ± 650 Da and the R_S is 29.2 ± 2.7 Å (see supplemental Fig. S1*C*). This value, although higher than the value expected for a folded trimer (21.6 Å), is nevertheless significantly lower than the value expected for an unfolded trimer (39 Å) (57). Notably, although the major peak is sharp and symmetric, a minor peak at 9.6 ml is also detectable (see supplemental Fig. S1*C*). The estimated molecular mass (~18 kDa) of this peak excludes the possibility that it might correspond to a dimer or a monomer.

The two-dimensional NOESY spectra of both P_{XD} proteins indicate that they are both folded, as judged from the spread of the resonance frequencies for amide protons and from the abundance of NOE signals in the amide-amide region (see Fig. 2*D* and supplemental Fig. S1*D*). The NOESY spectra also indicate that both NiV and HeV P_{XD} adopt a predominantly α-helical conformation, as judged from the upfield shifting of several HN chemical shifts (see Fig. 2*D* and supplemental Fig. S1*D*).

Binding of P_{XD} *to* N_{TAIL}—The ability of the X domains of both *Henipavirus* members to bind to N_{TAIL} was investigated by mixing purified N_{TAIL} and P_{XD} and analyzing complex formation by SEC-MALLS-RI. To this end, we incubated a fixed amount of N_{TAIL} (0.3 mM) with increasing concentrations of P_{XD} (0.3, 0.6, 0.9, and 1.2 mM) and then investigated complex formation using SEC-MALLS-RI. NiV and HeV N_{TAIL} domains were eluted at 8.1 and 8.2 ml, respectively, corresponding to an R_S of either 33.8 ± 2.4 Å (NiV) or 31.2 ± 2 Å (HeV). These values are consistent, within the error bar, with previous SEC and dynamic light scattering data (14) and are close to the theoretical value (28 Å) expected for monomeric PMG forms (57).

In the case of the study of the NiV N_{TAIL}-P_{XD} complex, upon addition of stoichiometric amounts of P_{XD}, the N_{TAIL} peak shifted toward a lower elution volume (from 8.1 to 7.75 ml), indicating the formation of an N_{TAIL}-P_{XD} complex, as also judged from the estimated mass (25,610 ± 80 Da), a value consistent with the binding of one P_{XD} molecule/N_{TAIL} (expected mass ~ 22 kDa) (data not shown). Upon adding a 2-fold molar excess of P_{XD}, no further significant shift in the elution volume of N_{TAIL} was observed, indicating that saturation was achieved for a 1:1 complex. Note however that under these conditions no

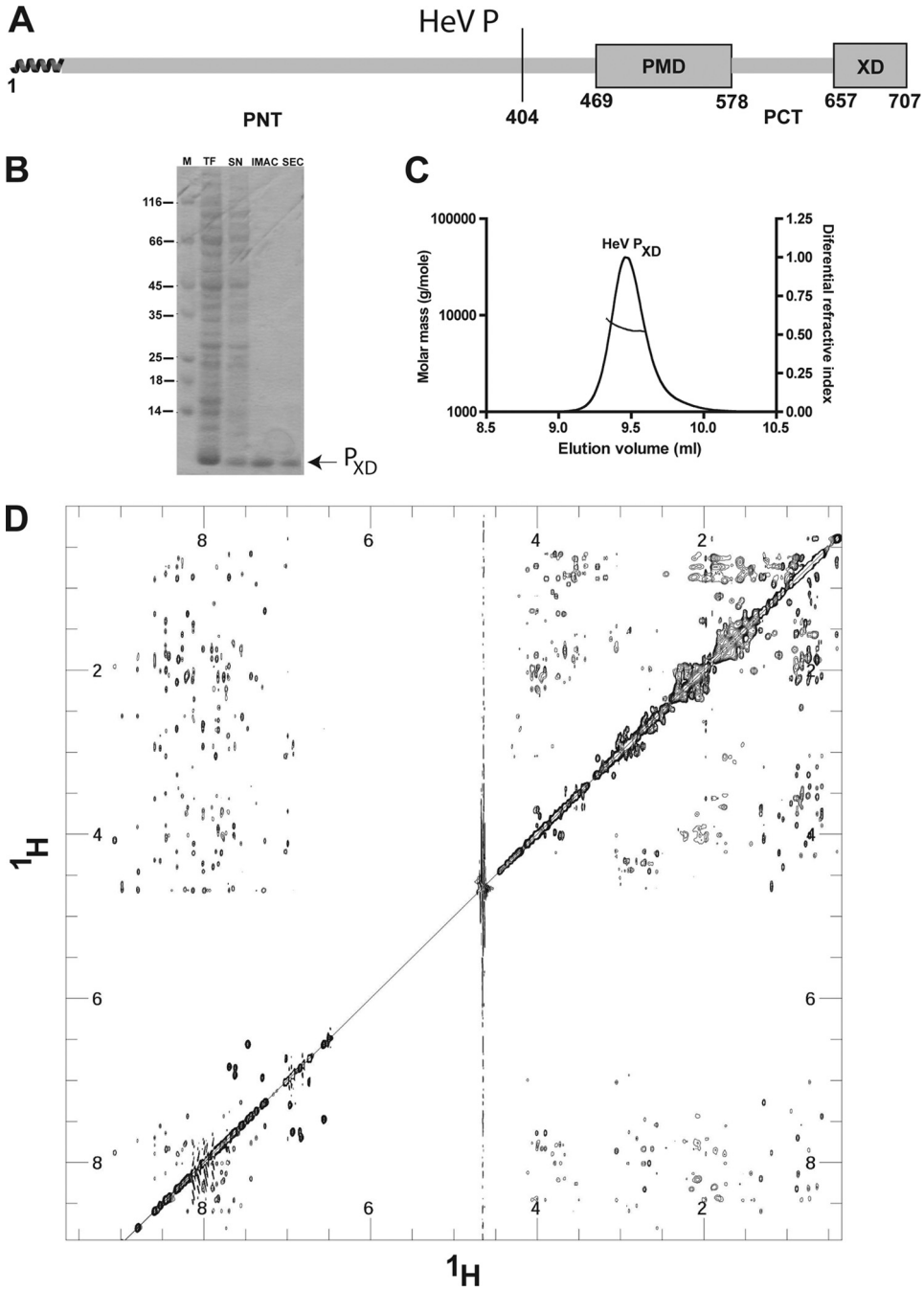

FIGURE 2. *A*, modular organization of HeV P according to Habchi *et al*. (14). The *large* and *narrow boxes* correspond to predicted structured and disordered regions, respectively. *PNT*, N-terminal disordered domain of P; *PMD*, P multimerization domain. *B*, 18% SDS-PAGE analysis of purified HeV P_{XD}. *TF*, total fraction; *SN*, soluble fraction; *IMAC*, eluent from IMAC; *SEC*, eluent from SEC; *M*, molecular mass markers. *C*, SEC-MALLS-RI analysis of purified HeV P_{XD}, where the *left y* axis represents the molecular mass and the *right y* axis represents the differential refractive index, with the *horizontal trace* showing the inferred molecular mass. *D*, two-dimensional NOESY spectrum of purified HeV P_{XD}.

peak corresponding to free P_{XD} was detected, with this latter becoming detectable only in mixtures containing a 3- or 4-fold molar excess of P_{XD} (see Fig. 3 and data not shown). The measured R_S of the complex is 35.4 ± 3.1 Å, a value larger than expected (22.3 Å) for a fully folded complex with a molecular mass equal to the sum of the masses of N_{TAIL} and P_{XD} (~22 kDa) (57), arguing for a complex that is not fully compact and hence retains a considerable flexibility.

Strikingly, in the case of the HeV N_{TAIL}-P_{XD} complex, the addition of P_{XD} molar excesses as high as 4 systematically resulted in no change in the elution profile of N_{TAIL} (data not shown). This indicated that under these experimental conditions no complex was formed, possibly reflecting a higher dissociation constant (K_D) for the HeV couple as compared with the NiV one.

ITC and SPR Studies—To estimate precisely the equilibrium dissociation constants and to ascertain possible differences in affinity between the two N_{TAIL}-P_{XD} complexes, the N_{TAIL}-P_{XD} binding reaction was further investigated by ITC, an approach that gives access to the stoichiometry, equilibrium association

constant, and variation in enthalpy and entropy (82). Purified *Henipavirus* N_{TAIL} domains were loaded into the calorimeter sample cell and titrated with the corresponding P_{XD}, achieving molar ratios of 2 (NiV pair) and 3.5 (HeV pair) at the end of the titration. The data, following integration and correction for the heats of dilution, were fit with a standard model allowing for a set of independent and equivalent binding sites (Fig. 4). The estimates for the model parameters (see Table 1) confirm a 1:1 stoichiometry and reveal that the binding reaction is both enthalpy- and entropy-driven, with the exception only of the NiV N_{TAIL}-P_{XD} couple for which a small unfavorable entropic contribution was found. The measured K_D was 2.1 ± 0.18 μM for the NiV pair and 8.7 ± 0.01 μM for the HeV pair. Similar experiments carried out in the presence of 1 M NaCl (data not shown) yielded similar results (see Table 1), suggesting that the N_{TAIL}-P_{XD} interaction relies mainly on hydrophobic interactions.

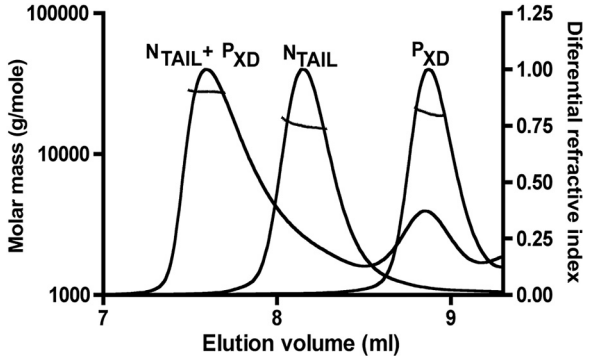

FIGURE 3. **SEC-MALLS-RI analysis of NiV N_{TAIL} and NiV P_{XD} and an N_{TAIL}/P_{XD} mixture containing a 4-fold molar excess of P_{XD}.** The *left y* axis represents the molecular mass, and the *right y* axis represents the differential refractive index. The *horizontal traces* show the molecular masses calculated from light-scattering intensity at different angles and differential refractive indexes as a function of the elution volume. The concentratio.ns of N_{TAIL} and P_{XD} were 0.3 and 1.2 mM, respectively.

In the case of NiV, we also studied the N_{TAIL}-P_{XD} interaction by SPR. Changes in SPR were monitored in real time as the NiV N_{TAIL} protein passed over sensor chips to which NiV P_{XD} was covalently coupled. Association and dissociation rates were found to be slow enough (k_{on} = 2.33 × 10^3 M^{-1} s^{-1}, k_{off} = 2.13 × 10^{-2} s^{-1}) to allow the equilibrium constant to be inferred from both kinetic and steady state analyses (see supplemental Fig. S2). Indeed, as specified by the manufacturer of the BIAcore 3000, good estimations of k_{on} and k_{off} can be calculated for the values in the range 10^3 to 10^6 M^{-1} s^{-1} and 10^{-5} to 10^{-2} s^{-1}, respectively. Binding affinities between P_{XD} and N_{TAIL} were established using 45–67 RU of immobilized P_{XD} and N_{TAIL} concentrations ranging from 0.1 to 50 μM (see "Experimental Procedures"). Dosage-dependent binding was observed in this range. The binding reaction conformed to a 1:1 ligand-substrate (Langmuir) binding model, exhibiting an excellent fit (*i.e.* $\chi^2 < 1$ and residuals within the range of ±2) following global kinetic analysis of sensorgrams as well as when plotting mean equilibrium responses of the data in the steady state analysis. The equilibrium dissociation constant (K_D) derived from the kinetic analysis was 9.1 μM, and the value derived from the steady state analysis was 7.3 μM (see Table 2), in good agreement with that measured by ITC (*cf.* Tables 1 and 2).

Induced Folding of Henipavirus N_{TAIL} in the presence of P_{XD}— The N_{TAIL} domains from the closely related MeV and Sendai

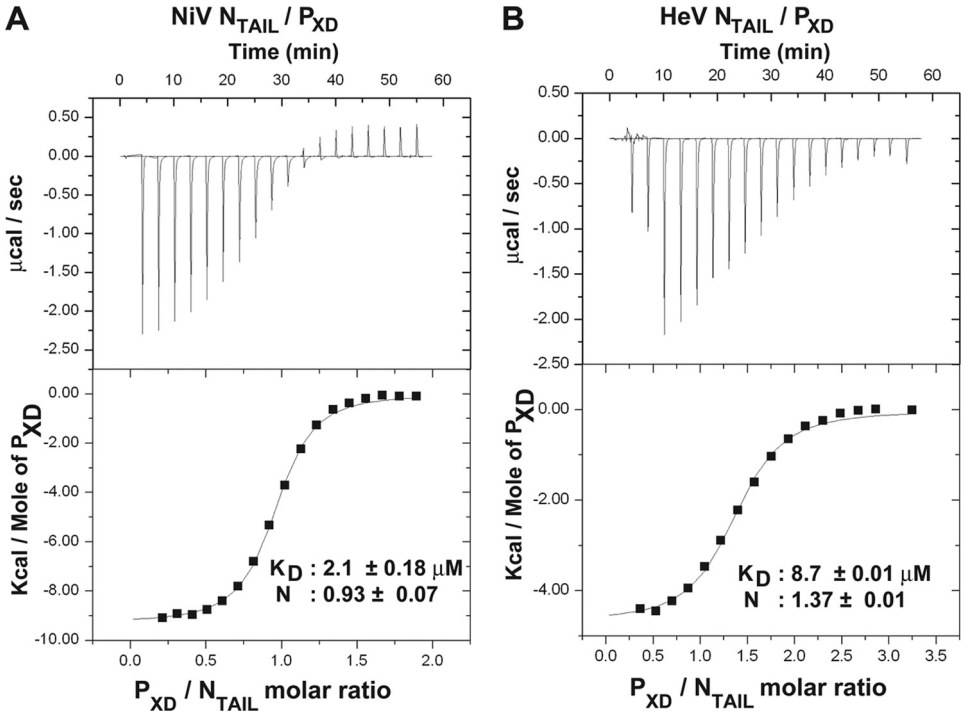

FIGURE 4. **ITC studies of NiV (*A*) and HeV (*B*) N_{TAIL}-P_{XD} complex formation.** Data are representative of three independent experiments in which the initial concentrations of N_{TAIL} in the microcalorimeter cell and of P_{XD} in the microsyringe were slightly tuned. Shown are data obtained with the following initial concentrations: 150 μM N_{TAIL} and 1.65 mM P_{XD} for NiV and 130 μM N_{TAIL} and 2.2 mM P_{XD} for HeV. Graphs shown at the *bottom* of each panel correspond to integrated and corrected ITC data fit to a single set of sites model (all sites are identical and equivalent). The *filled squares* represent the experimental data, and the *solid lines* corresponds to the model.

TABLE 1

Equilibrium dissociation constants and binding parameters for both *Henipavirus* N_{TAIL}-P_{XD} complex formations as derived from ITC studies

Data are representative of three independent trials.

	Stoichiometry	K_D (μM)	Binding enthalpy ΔH	Binding entropy ΔS
	n		*cal mol*$^{-1}$	*cal mol*$^{-1}$ *deg*$^{-1}$
NiV *wt* N_{TAIL}-NiV P_{XD} 0.2 M NaCl	0.93 ± 0.07	2.1 ± 0.18 μM	−9034 ± 108.9	−4.84
NiV *wt* N_{TAIL}-NiV P_{XD} 1 M NaCl	1.30 ± 0.05	10 ± 0.33 μM	−2649 ± 160.2	13.8
NiV N_{TAIL} F527W-NiV P_{XD} 0.2 NaCl	0.97 ± 0.02	5.6 ± 0.32 μM	−2887 ± 78.9	14.2
HeV *wt* N_{TAIL}-HeV P_{XD} 0.2 M NaCl	1.37 ± 0.01	8.7 ± 0.01 μM	−5584 ± 62	4.09
HeV *wt* N_{TAIL}-HeV P_{XD} 1 M NaCl	1.31 ± 0.04	11.5 ± 0.51 μM	−1025 ± 43.2	19.1
HeV N_{TAIL} F527W-HeV P_{XD} 0.2 NaCl	0.85 ± 0.02	6.9 ± 0.4 μM	−3813 ± 143	10.6

TABLE 2

Kinetic and steady state parameters for the NiV N_{TAIL}-NiV P_{XD} binding reaction

Data are representative of two trials.

	Quality of fit				
	Residuals	Chi^2	k_{on}	k_{off}	K_D
			M^{-1} s^{-1}	s^{-1}	μM
Global	−0.6–0.75	0.0459	2.33×10^3	2.13×10^{-2}	9.1
Steady state	0.039	0.865			7.3

virus (SeV) have been shown previously to undergo α-helical induced folding in the presence of the cognate X domains (44–55, 83, 84). To investigate whether *Henipavirus* N_{TAIL} domains undergo induced folding in the presence of P_{XD} either, we used far-UV CD spectroscopy.

As expected from the NOESY spectra, the far-UV CD spectra of both P_{XD} proteins (Fig. 5, *A* and *B*, *gray lines*) are typical of structured proteins with a predominant α-helical content, indicated by the positive ellipticity between 190 and 200 nm and by the two minima at 208 and 222 nm. Conversely, the CD spectra of both N_{TAIL} proteins are typical of predominantly unfolded proteins, as seen by their large negative ellipticity at 198 nm and low ellipticity at 190 nm (Fig. 5, *A* and *B*, *black lines*). Nevertheless, and as already reported (14), the observed ellipticity values at 200 and 222 nm of both *Henipavirus* N_{TAIL} proteins are consistent with the existence of some residual secondary structure typical of IDPs adopting a PMG conformation (21). To each N_{TAIL} domain we added a 2-fold molar excess of the corresponding P_{XD}. Under these experimental conditions, the N_{TAIL} and P_{XD} concentrations (350 and 700 μM, respectively) were well above the estimated K_D and hence were expected to lead to 100% complex formation. Indeed, the observed CD spectra of the mixtures differed from the corresponding theoretical average curves calculated from the individual N_{TAIL} and P_{XD} spectra (Fig. 5). As the theoretical average curves correspond to the spectra that would be expected if no structural variations occur, deviations from these curves indicate structural transitions. The experimentally observed spectra of the mixtures support a random-coil to α-helix transition, as judged by the much more pronounced minima at 208 and 222 nm and by the higher ellipticity at 190 nm of the experimentally observed spectra compared with the corresponding theoretical average curves (see Fig. 5, *A* and *B*). In particular, (i) the experimental CD spectra of the mixtures deviate considerably from the average curves in the 190–195 region, with this deviation being more pronounced in the case of the HeV N_{TAIL} + P_{XD} mixture; and (ii) mixture spectra display a pronounced decrease in the ellipticity at 208 and 222 nm with respect to the average curves, with this decrease being more significant in the case of the NiV N_{TAIL} + P_{XD} mixture (Fig. 5, *A* and *B*). A quantitative analysis of the spectra (see "Experimental Procedures") allowed an estimation of the percentages of α-helical and disordered structure in all of the spectra (Fig. 5, *C* and *D*). This analysis indicated a significant increase in the α-helical content of the mixtures as compared with average spectra, with this gain in α-helicity being paralleled by a decrease in the content of disordered structure (see Fig. 5, *C* and *D*). As a control, we recorded the CD spectra of both N_{TAIL} in the presence of a 2-fold molar excess of lysozyme (data not shown). The absence of significant structural variations in the presence of lysozyme confirms the specificity of the deviations observed upon the addition of P_{XD} to the corresponding N_{TAIL} protein.

Two-dimensional Heteronuclear Nuclear Magnetic Resonance Titration Studies—To further explore the nature of the interaction established by *Henipavirus* N_{TAIL} and P_{XD}, we used NMR spectroscopy. We recorded the HSQC spectra of uniformly ^{15}N labeled N_{TAIL} before and after the addition of increasing amounts of unlabeled P_{XD}. These studies, by allowing chemical shift changes in the backbone amide and proton resonances to be followed upon the addition of unlabeled P_{XD}, yielded an estimation of the number of N_{TAIL} residues involved in the interaction with P_{XD}. For both titrations, most resonances in the HSQC experienced no chemical shift changes, and only a few resonances underwent fast to intermediate exchange (Fig. 6 and supplemental Fig. S3). Saturation (*i.e.* no changes in chemical shifts upon further addition of the partner to ^{15}N-labeled N_{TAIL}) was achieved with N_{TAIL}:P_{XD} molar ratios of 1:1.75 and 1:1.56 for NiV and HeV N_{TAIL}, respectively. This finding is in line with what could be expected from the experimentally determined dissociation constants, from which the percentage of bound N_{TAIL} was estimated to be 80% in the case of the HeV titration and 100% for that of NiV.

In the case of HeV N_{TAIL}, ~100 peaks were detectable in the HSQC, including the 10 expected N_{TAIL} glycines and at least 18 Ser/Thr residues (see supplemental Fig. S3). Following the addition of P_{XD}, around 15 peaks disappeared from the spec-

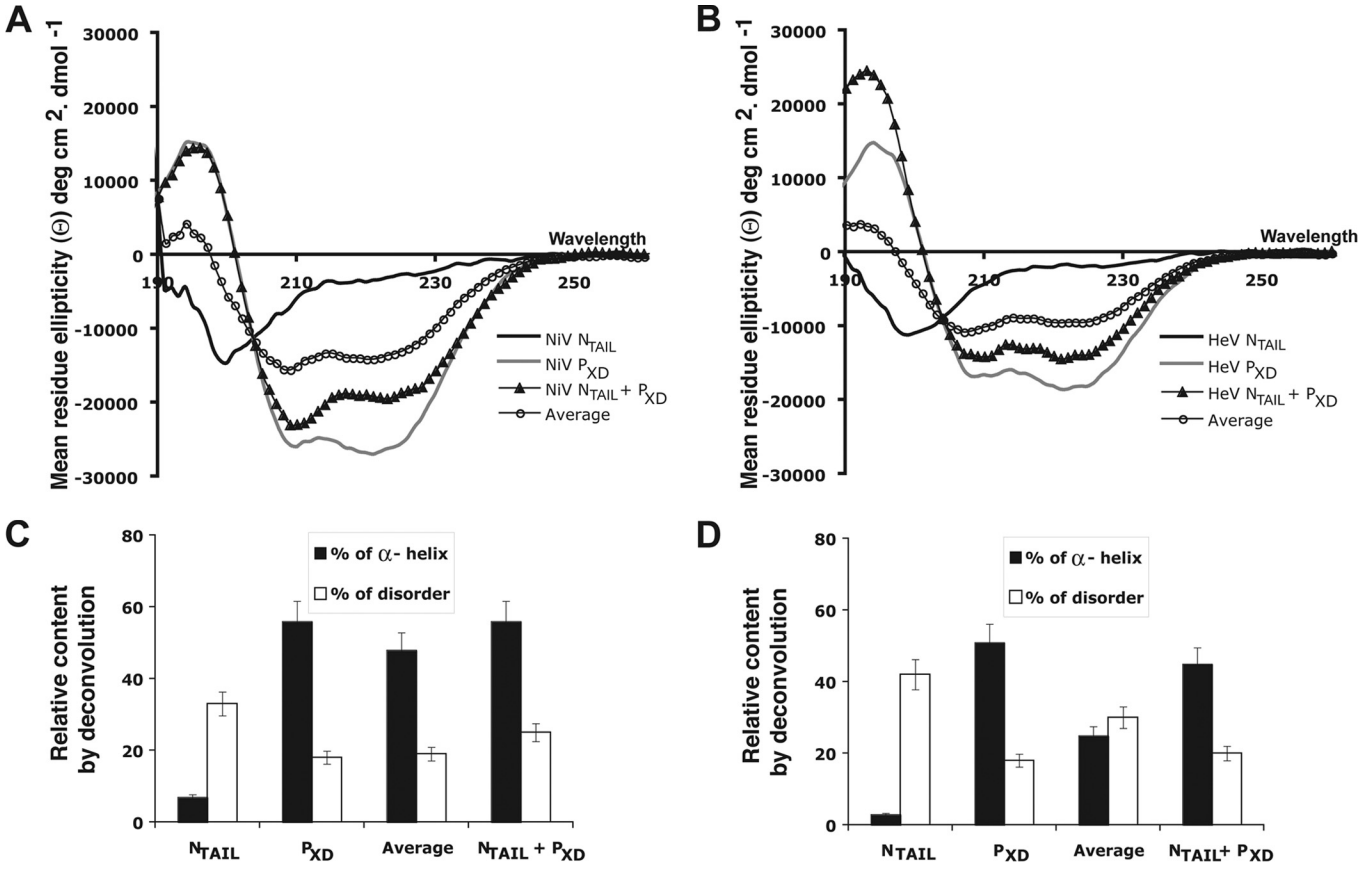

FIGURE 5. *A* and *B*, far-UV CD studies of NiV N_{TAIL} (*A*) and HeV N_{TAIL} (*B*) either alone (*black line*) or in the presence of a 2-fold molar excess of P_{XD} (*filled triangles*). The CD spectrum of P_{XD} alone (*gray line*) and the theoretical average curves (*empty circles*) calculated by assuming that no structural variations occur (see "Experimental Procedures") are also shown. *C* and *D*, estimated content in α-helix and unordered structure of each NiV (*C*) and HeV (*D*) spectrum as obtained using DichroWeb (see "Experimental Procedures"). The *error bar* (10% of the value) corresponds to the experimentally determined S.D. from three independent experiments. Spectra were recorded at 20 °C in 10 mM Tris/HCl, pH 7.5, NaCl 200 mM. In the mixture containing N_{TAIL} + P_{XD}, the concentration of N_{TAIL} was 350 μM, and that of P_{XD} was 700 μM. The path length was 0.01 mm. Data are representative of one of three independent experiments.

trum of N_{TAIL}, consistent with an intermediate exchange regime (*i.e.* the exchange rate between free and bound N_{TAIL} is comparable with the chemical shift difference between the free and the bound forms). The 15 residues that disappeared do not imply any Gly but include 4–5 Ser/Thr. Notably, even with P_{XD} molar ratios as high as 8.5, no new peaks reappeared corresponding to the fully bound form of N_{TAIL} (see supplemental Fig. S3) nor could they be observed upon further increasing the molar excess of P_{XD} up to 13 (data not shown). In addition, 3–4 peaks (including 2 of the 10 glycines) showed chemical shift changes upon the addition of P_{XD} according to a fast to intermediate exchange regime (see supplemental Fig. S3). These observations could be accounted for by assuming that P_{XD} binds to N_{TAIL} in close proximity of the α-MoRE predicted to encompass residues 473–493, although other binding scenarios cannot be ruled out.

In the case of NiV N_{TAIL}, similar results were obtained (Fig. 6). The peaks that disappeared upon the addition of P_{XD} imply 5–6 Ser/Thr (see Fig. 6*A*), and at least two peaks underwent fast to intermediate exchange (see Fig. 6, *A* and *B*). We also performed a quantitative analysis of the NMR titration data. We plotted the chemical shift variation as a function of the partner molar ratio for those peaks that undergo fast exchange (see Fig. 6*C*). When applied to the peak shown in Fig. 6*B*, this analysis yielded an apparent dissociation constant (K_{Dapp}) of 2 ± 0.06 μM, a value in very good agreement with the K_D determined by both ITC and SPR studies. A very similar K_{Dapp} value (5 ± 0.2 μM) was obtained by performing this quantitative analysis on another similarly behaving peak (data not shown). Interestingly, in the case of the NiV N_{TAIL} titration, but not of the HeV one, among the correlation peaks that were displaced by P_{XD}, eight underwent an upfield shift (see Fig. 6*A*) consistent with a random coil to α-helix transition.

In conclusion, these experiments revealed that complex formation between N_{TAIL} and P_{XD} implies both fast and intermediate exchange. In addition, in the case of NiV, binding to P_{XD} triggers a gain of α-helicity for at least eight residues.

Generation of Single-site Trp N_{TAIL} Variants and Fluorescence Spectroscopy Studies—To assess the possible contribution of the C-terminal region of N_{TAIL} to binding to P_{XD}, we designed a single-site Trp variant for both NiV and HeV N_{TAIL} in view of intrinsic fluorescence studies. For both NiV and HeV N_{TAIL} we targeted a unique, naturally occurring aromatic residue (Phe-527) and generated an N-terminally hexahistidine-tagged N_{TAIL} variant (referred to as N_{TAIL} F527W) bearing the F527W substitution. Introduction of a tryptophan residue in both N_{TAIL} domains was conceived to allow binding events to be followed by fluorescence spectroscopy while maximizing the

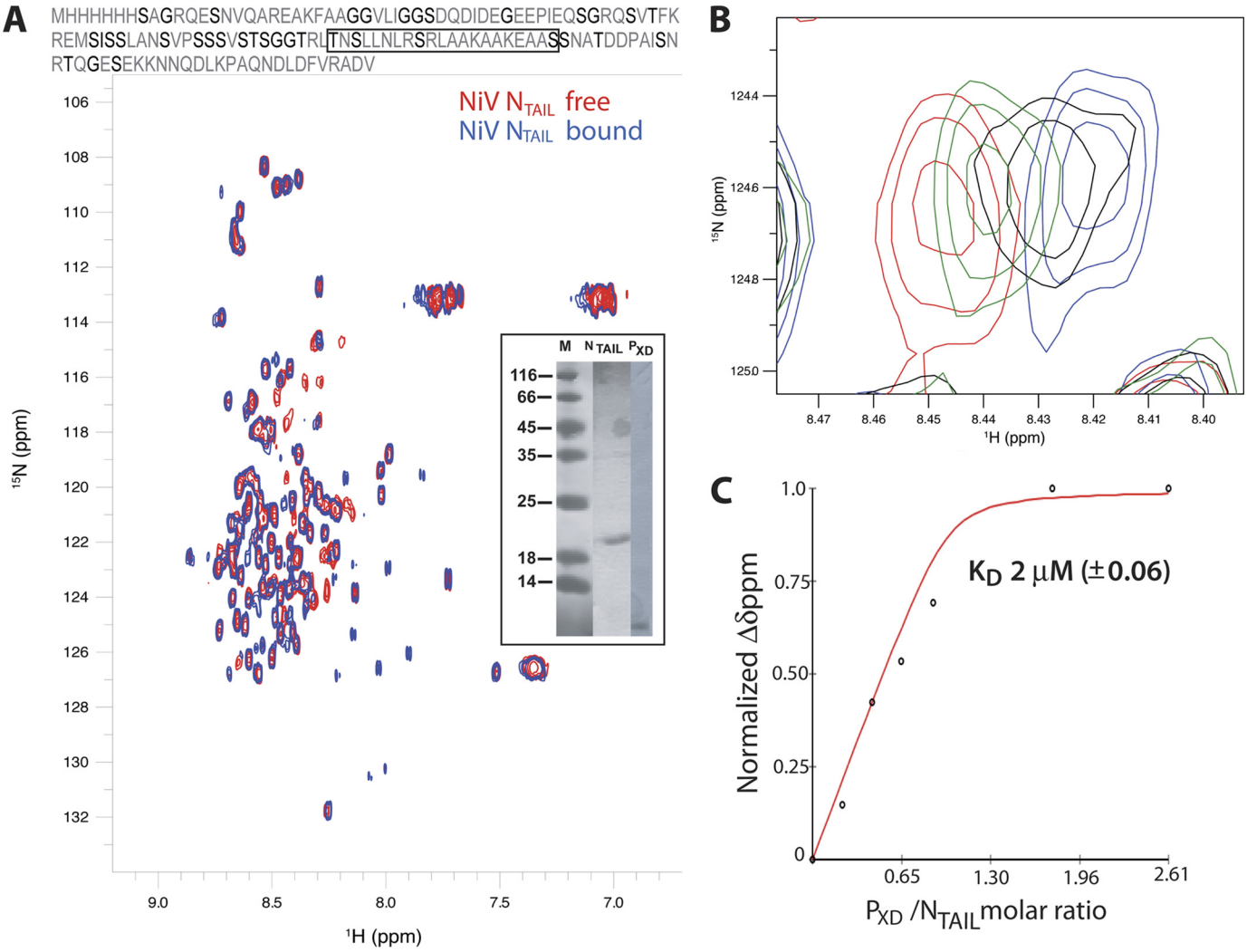

FIGURE 6. *A*, 2D-HSQC spectrum of purified NiV ^{15}N N_{TAIL} either alone (*red*) or in the presence (*blue*) of saturating amounts of P_{XD} (P_{XD}/N_{TAIL} molar ratio = 2.63). The amino acid sequence of NiV N_{TAIL} is shown above the spectra, with Gly and Thr/Ser residues shown in *bold letters*. The predicted α-MoRE encompassing residues 473–493 is *framed*. The *inset* shows purified NiV ^{15}N-N_{TAIL} and P_{XD}. *B*, changes in the chemical shift of the backbone amide ^{15}N resonance of one NiV N_{TAIL} peak in fast exchange during the titration. Bound and free chemical shift positions are indicated in *blue* and *red*, respectively. The positions obtained with N_{TAIL}:P_{XD} molar ratios of 1:0.219 and of 1:0.657 are shown in *green* and *black*, respectively. Note that saturation was achieved for a 1:1 complex. *C*, chemical shift variations of the backbone amide ^{15}N resonance of the peak shown in *B* as a function of P_{XD} molar excess. The *solid line* represents the fitted model. All spectra were recorded at 283 K. *ppm*, quotes for resonance shifts in parts per million of the spectrophotometer frequency.

conservative nature of the substitution (note that the two X domains contain no tryptophan residues).

Both NiV and HeV N_{TAIL} F527W variants were purified from the soluble fraction of the bacterial lysate by IMAC and preparative SEC (see Fig. 7, *A* and *B*, *insets*). The identity of the recombinant products was confirmed by mass spectrometry analysis of tryptic digests of fragments obtained after digestion of the purified proteins excised from SDS-polyacrylamide gels (data not shown). Both N_{TAIL} proteins display an abnormally slow migration in SDS-PAGE with an apparent molecular mass of 20 kDa (expected MM 15 kDa) (see Fig. 7, *A* and *B*, *insets*). This abnormal migratory behavior has already been documented for both native N_{TAIL} domains, where mass spectrometry analyses gave the expected results (14). Hence, this anomalous electrophoretic mobility is rather due to a rather high content of acidic residues, as already observed for other intrinsically disordered domains (for examples see Ref. 6, 45, and 85) and, more generally, in other IDPs (86). Indeed, because of their biased amino acid composition, often leading to enrichment in negatively charged residues, IDPs bind less SDS than naturally folded proteins. As a result, their apparent molecular mass is often 1.2–1.8 times higher than the real one calculated from sequence data or measured by mass spectrometry (86).

Both N_{TAIL} variants displayed the same SEC elution profile as the *wt* form (data not shown), being eluted from a Superdex S200 column as sharp peaks with an apparent molecular mass (43 kDa) well above the expected one and leading to an estimated R_S of 28 ± 2 Å (see "Experimental Procedures"). Note that the elution behavior was found to be buffer-independent, as the same elution profiles were obtained regardless of whether a sodium phosphate or Tris/HCl buffer was used for elution and irrespective of the NaCl concentration. Thus, both variants exhibit hydrodynamic properties similar to those of the *wt* forms, suggesting that they both adopt a PMG conformation. In further support of this observation, the far-UV CD spectra of N_{TAIL} F527W proteins are typical of predominantly unfolded

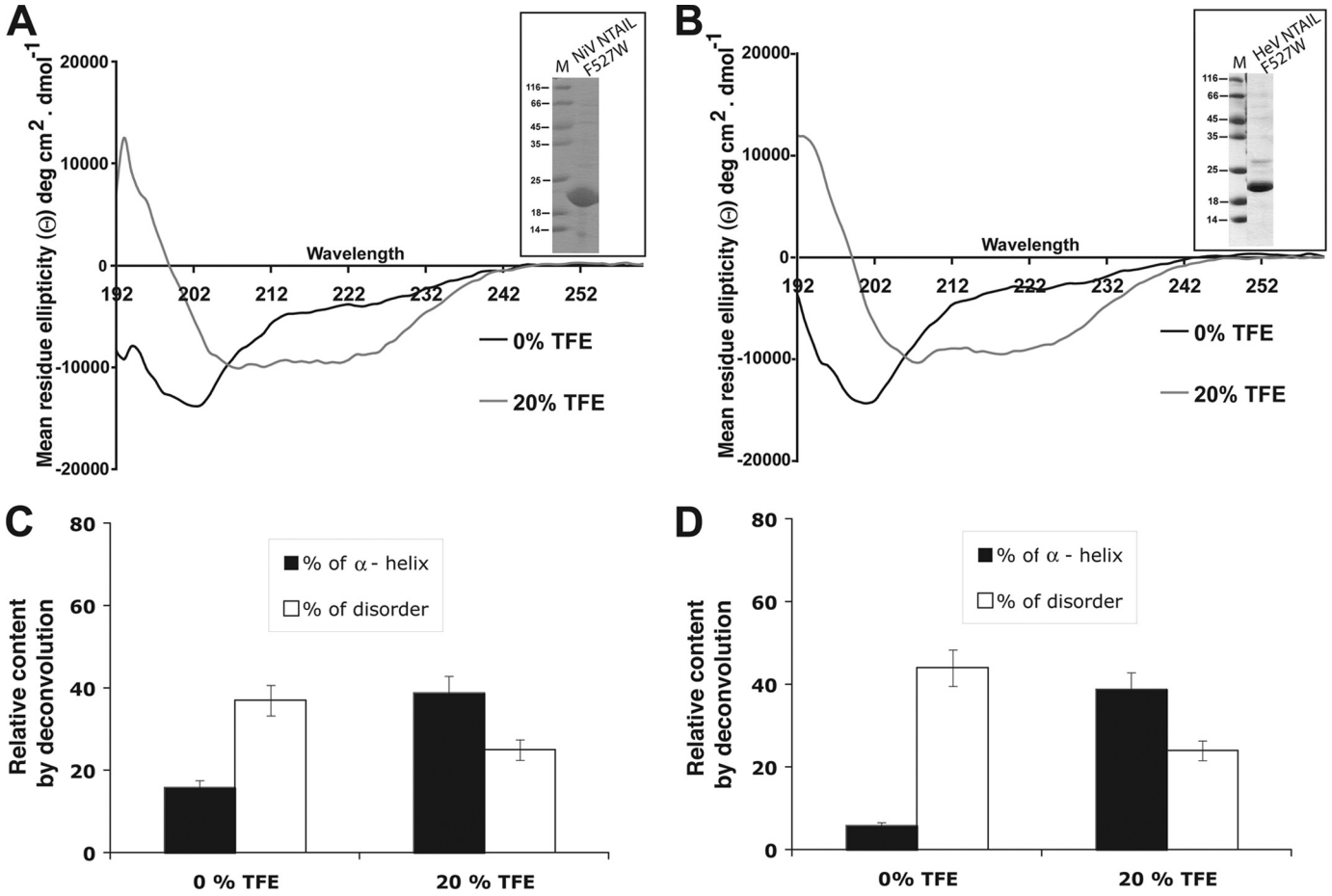

FIGURE 7. *A* and *B*, far-UV CD spectra of NiV (*A*) and HeV (*B*) N_{TAIL} F527W recorded at 20 °C in 10 mM sodium phosphate buffer, pH 7, either in the absence or presence of 20% TFE. The protein concentration was 0.1 mg/ml, and the path length was 1 mm. The *insets* show a 15% SDS-PAGE analysis of the purified proteins. *C* and *D*, estimated content in α-helix and unordered structure of each NiV (*C*) and HeV (*D*) spectrum as obtained using DichroWeb (see "Experimental Procedures"). The *error bar* (10% of the value) corresponds to the experimentally determined S.D. from three independent experiments.

forms devoid of stable, highly populated secondary structure (see Fig. 7, *A* and *B*) and are almost perfectly superimposable on those of both native N_{TAIL} domains (data not shown). These observations indicate that the tryptophan residue does not affect the overall secondary structure content of the protein. To test the potential of both N_{TAIL} variants to undergo folding, we recorded their CD spectra in the presence of 20% TFE, a condition where both *Henipavirus wt* N_{TAIL} proteins undergo dramatic structural transitions (14) (Fig. 7, *A* and *B*). The solvent TFE is widely used as an empirical probe of hidden structural propensities of peptides and proteins, as it mimics the hydrophobic environment experienced by proteins in protein-protein interactions (87–89). Both proteins show an increasing gain of α-helicity upon the addition of TFE, as indicated by the characteristic maximum at 190 nm and double minima at 208 and 222 nm (Fig. 7, *A* and *B*). Under these conditions, the α-helicity was estimated to be ~40% for both variants (see Fig. 7, *C* and *D*), a value close to that observed for both native N_{TAIL} domains (14). These results indicate that the Phe to Trp substitution does not affect the folding abilities of the two N_{TAIL} variants, thus supporting their biochemical relevance. That the single-site Trp variants behave like the native forms was also demonstrated by ITC studies showing that the variants bind to P_{XD} with K_D values close to those observed with the *wt* N_{TAIL} forms (Table 1).

Fluorescence spectroscopy studies showed that the NiV variant has a maximum of emission at 351 nm, while the maximum of emission of the HeV variant is at 355 nm, indicating that in both N_{TAIL} variants the Trp-527 is fully exposed to the solvent. The addition of gradually increasing P_{XD} molar excesses (up to 60) did not trigger any coherent, dose-dependent increase or decrease in the fluorescence intensity (data not shown), nor did it cause any significant shift in the emission maximum (see supplemental Fig. S4). Because in these studies the N_{TAIL} and P_{XD} concentrations in the course of the titration were well above the estimated K_D, these results argue for the lack of significant variations in the chemical environment of the unique Trp residue at position 527 upon P_{XD} binding.

Structural Models of Henipavirus N_{TAIL}-P_{XD} *Complexes*—NMR titration studies suggested that P_{XD} might bind to an N_{TAIL} region close to the predicted α-MoRE spanning residues 473–493, an hypothesis also supported by previous studies carried out by others showing that P binds to residues 468–496 of N (12, 13). In addition, both NMR and far-UV CD studies revealed a gain of α-helicity within N_{TAIL} upon binding to P_{XD}, and ITC studies showed that the interaction does not rely on

electrostatic contacts, as the K_D was not affected by NaCl concentrations as high as 1 M. On the other hand, fluorescence spectroscopy studies indicated a lack of impact of P_{XD} on a Trp residue at position 527 of N_{TAIL}, arguing for the lack of stable contacts between the region in close proximity to this Trp residue and P_{XD}. On the basis of all of these considerations, and also by analogy with the related MeV, we built a model of the N_{TAIL}-P_{XD} complex involving the α-MoRE encompassing residues 473–493 and implying hydrophobic contacts.

The structural models of both NiV and HeV P_{XD} were obtained using the SAM-06 server. In both cases, the crystal structure of P_{XD} from the related MeV (PDB code 1OKS) (44) was found to be the best hit, with E-values of 5.333 e^{-3} (NiV) and 2.257 e^{-2} (HeV). Note that an automated search of the PDB database (90) for homologous structures using either the ESyPred3D (91) or the Swiss-Model (92) servers failed to generate a structural model, as the sequence identity between either HeV or NiV P_{XD} and MeV P_{XD} (19.6 and 15.7%, respectively) is lower than the threshold used by these servers.

The α-MoRE encompassing residues 473–493 in both *Henipavirus* N_{TAIL} domains can be modeled as an α-helix with one side mostly hydrophobic. After having obtained the structural model of both P_{XD} proteins, we modeled the α-helical α-MoRE of N_{TAIL} in the hydrophobic cleft delimited by helices α2 and α3 of P_{XD} to yield a pseudo-four-helix arrangement similar to that already observed for the closely related MeV N_{TAIL}-P_{XD} complex (74) (Fig. 8).

After energy minimization and manual refinement, a good shape complementarity between the α-MoRE and P_{XD} was observed for both *Henipavirus* complexes. For the final structural model of the NiV complex, 98.5% of the residues were found to lie in the favorable region of the Ramachandran plot, with a final MolProbity score of 1.77 and an overall clashscore of 18.6. For the final structural model of the HeV complex, 98.5% of the residues were found to lie in the favorable region of the Ramachandran plot, with a final MolProbity score of 1.76 and an overall clashscore of 18.4.

The resulting models are loosely packed, with an interface area of 439 $Å^2$ for the NiV complex and 337 $Å^2$ for the HeV complex. The HeV complex is stabilized by hydrophobic interactions between side chain carbon atoms of the interacting pairs P Ile-702/N Ile-488 and P Tyr-682/N Ala-484, as well as by a hydrogen bond between the backbone oxygen of P Asp-681 and the NH1 group of N Arg-480. The NiV complex is stabilized by a hydrogen bond between the backbone oxygen of P Lys-687 and the NH1 group of N Arg-480 and by several hydrophobic contacts involving side chain atoms from the interacting pairs P Ala-688/N Leu-477, P Ile-697/N Ala-484, P Ile-704/N Ala-488, and P Ile-704/N Ala-491.

The final structural models are quite close to the structure of the MeV template; for the NiV complex, the pairwise r.m.s.d. is 0.67 Å for the P_{XD} chain (over 47 aligned residues out of 50) and 0.79 Å (over 18 aligned residues out of 21) for the α-MoRE. In the case of the HeV complex, the pairwise r.m.s.d. is 2.0 Å (over 46 aligned residues out of 51) for P_{XD} and 0.68 Å (over 18 aligned residues out of 20) for the α-MoRE. The most significant structural differences concern the loop between helices α2 and α3 of HeV P_{XD}, with the maximal deviation occurring between MeV Lys-489 and HeV Asp-687 (Cα distance of 5.2 Å). In the case of the NiV complex, this loop deviates much less from that of MeV P_{XD}, and the maximal deviation between the two models concerns the α-MoRE, with a Cα distance of 4.4 Å between NiV N Asn-474 and MeV N Asp-487.

DISCUSSION

Henipavirus N Proteins Form Nucleocapsid-like Particles in Which the N_{TAIL} Domain Is Disordered—The SEC profile of *Henipavirus* N proteins, together with their A_{260}/A_{280} ratio, supports the formation of nucleocapsid-like particles upon expression in *E. coli*, in agreement with previous findings showing that NiV N self-oligomerizes upon expression in insect cells (80) and forms speckles in live transfected BHK cells (13) in accordance with the general behavior of nucleoproteins from Mononegavirales members.

In a previous study, by combining computational and biochemical approaches, we showed that both NiV and HeV N_{TAIL} domains are mostly unstructured in solution although they contain some residual, transiently populated, secondary structure (14). Whether these domains were also disordered in the context of the full-length nucleoproteins was however still a matter of debate. Herein we used limited proteolysis to address the disordered state of N_{TAIL} within the entire N proteins. Because disordered regions are highly sensitive to proteolysis, limited proteolysis is a powerful tool for investigating protein structural properties (see Refs. 93–95 and 96 and references cited therein). The results presented here show that both N proteins undergo proteolytic cleavage within their N_{TAIL} domains, thus supporting the disordered nature of these domains not only in isolation but also in the context of the entire N proteins.

The X Domains of Henipavirus P Proteins Are Autonomously Folding Units Adopting an α-Helical Conformation—Previous bioinformatics analyses by our laboratory allowed us to propose a modular organization of *Henipavirus* P and to designate the X terminal domain as a putative globular domain that, by analogy with the closely related MeV, might interact with *Henipavirus* N_{TAIL}. We therefore targeted both NiV and HeV P_{XD} for expression in *E. coli*. Indeed, both X domains were found to be expressed in the soluble fraction of the bacterial lysate, suggesting that P_{XD} do represent *bona fide* domains, *i.e.* autonomously folding units. In further support of this observation, both CD and NMR studies showed that both of the P X domains are folded and adopt a predominantly α-helical conformation. Strikingly, although HeV P_{XD} was found to be monomeric and eluted as a unique, very sharp peak, NiV P_{XD} was found to be trimeric and eluted in two peaks: a major, very sharp peak and a minor peak in which the estimated molecular mass is consistent with a trimeric form possibly adopting a slightly more compact conformation. The possibility that the major elution peak of NiV P_{XD} might correspond to a monomeric form adopting a molten globule conformation, as in the case of the C-terminal X domain of the mumps virus (97, 98), was checked and ruled out by NMR studies, where the NOESY spectrum clearly showed that the NiV P_{XD} is folded. Whatever the origin of the minor elution peak, it is noteworthy that the slight heterogeneity of NiV P_{XD} did not, however, impair complex formation with N_{TAIL}.

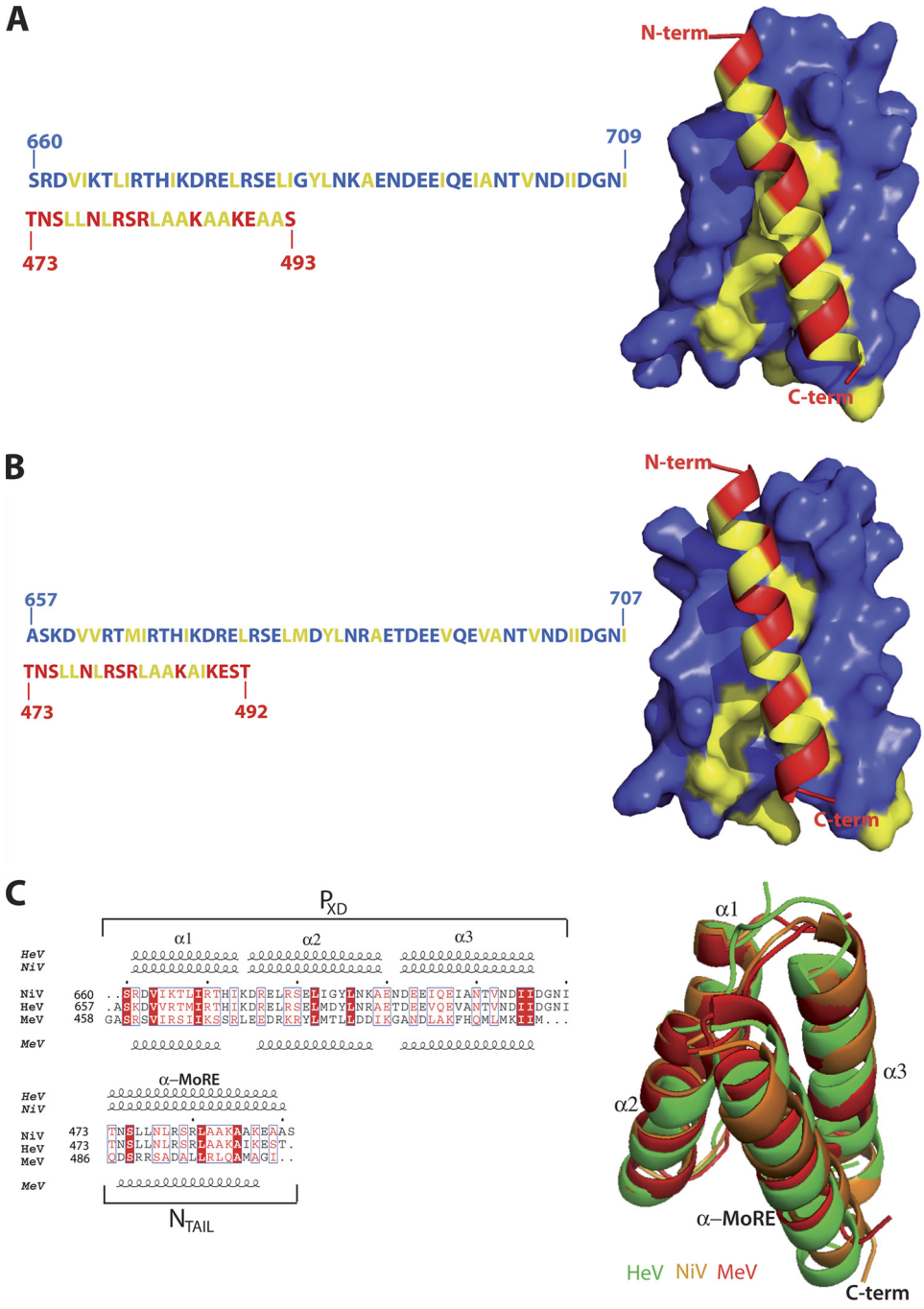

FIGURE 8. *A* and *B*, structural models of the NiV (*A*) and HeV (*B*) complexes between P_{XD} and the N_{TAIL} region predicted to adopt an α-helical conformation (amino acids 473–493 for NiV and 473–492 for HeV) within a predicted N_{TAIL} α-MoRE. P_{XD} is shown in *blue* with surface representation, and the α-MoRE of N_{TAIL} is shown in *red* in ribbon representation. Hydrophobic residues are shown in *yellow*. The amino acid sequence of P_{XD} and of the N_{TAIL} region that was modeled in the complex is shown with the same color code. *C*, superimposition of the structural models (ribbon representation) of the P_{XD}-N_{TAIL} complexes of HeV (*green*) and NiV (*orange*) onto the crystal structure of a MeV chimeric construct (*red*) encompassing P_{XD} (amino acids 459–507 of P) and residues 486–504 of N (PDB code 1T6O) (74). A multiple sequence alignment of *Henipavirus* and MeV P_{XD} as obtained using ClustalW and ESPript is also shown. Residues corresponding to a similarity greater than 60% are *boxed* and shown in *red*. Identical residues are *boxed* and shown in *white* on a *red background*. The *numbers* written in *front* of the sequences correspond to the amino acid positions in the P and N sequences. *Dots* above the alignment indicate intervals of 10 residues. Predicted secondary structure elements of HeV and NiV P_{XD}, as obtained using the PSIPRED server, are shown *above* the multiple sequence alignment. Secondary structure elements, as observed in the crystal structure of the MeV chimeric construct (PDB code 1T6O) are shown *below* the alignment. All structural models were drawn using PyMOL (79).

Our ability to obtain large amounts of purified P_{XD}, beyond validating the reliability of the prediction of the modular organization of *Henipavirus* P, highlights the general interest of a domain approach for the biochemical and structural study of viral proteins. This has already been well illustrated in the case of the P proteins from measles (44) and Sendai viruses (83, 99–102) as well as for the phosphoproteins from Rhabdoviridae members (103–107), and, more generally, for viral proteins targeted by large scale structural genomics projects (for examples see Refs. 108–116).

The X Domains of Henipavirus P Proteins Bind to the Intrinsically Disordered N_{TAIL} Domains and Form a 1:1 Complex—Although NiV P_{XD} was found to be trimeric, SEC-MALLS studies indicated that this latter binds to N_{TAIL} as a monomer, as judged from the molecular mass (~25 kDa) of the observed N_{TAIL}-P_{XD} complex. The lack of detection of free P_{XD} in the N_{TAIL}:P_{XD} mixture containing a 2-fold molar excess of P_{XD} likely arises from the limited resolution of the KW-802.5 SEC column for small protein molecules, where these latter can escape detection unless they are highly concentrated. Accordingly, a peak corresponding to free (trimeric) P_{XD} becomes detectable in mixtures with P_{XD} concentrations of 0.9–1.2 mM. The fact that the elution volume of the NiV N_{TAIL}-P_{XD} complex remains the same, even with P_{XD} molar excesses as high as 4, could be accounted for by either the formation of a 1:1 stoichiometric complex or by a more complex binding scenario in which binding of the first P_{XD} molecule would occur with a relatively high affinity, whereas putative binding of additional P_{XD} molecules would be governed by a much lower affinity. This latter hypothesis is rather unlikely, however, as it would imply a K_D higher than the highest P_{XD} concentration used in these studies (1.2 mM) and would hence not be physiologically relevant. In further support of the first binding scenario, formation of a 1:1 complex was further confirmed by both ITC and SPR studies that also revealed a K_D in the μM range for both complexes.

Surprisingly, in the case of HeV, SEC-MALLS studies failed to unveil complex formation, as no shift in the elution volume of N_{TAIL} was observed even with P_{XD} molar excesses as high as 4. These findings are puzzling, because these experiments were carried out under the same buffer conditions used for the ITC studies, which not only clearly revealed the formation of a 1:1 complex but also indicated a K_D comparable with that observed for the NiV N_{TAIL}-P_{XD} binding reaction. Because detection of protein complexes by SEC is notoriously challenging for complexes characterized by K_D in the μM range, these results might reflect more subtle differences between the HeV and NiV complexes, despite the similar K_D values. That the two complexes do behave differently is further supported by the different HeV N_{TAIL} resonance behavior in titration studies with respect to NiV N_{TAIL}, as well as by the smaller interface of the HeV complex, as judged from the structural models (for a more detailed discussion of these two points, see below).

Binding to P X Domains Triggers α-Helical Folding of the Intrinsically Disordered N_{TAIL} Domains—Far-UV CD spectroscopy has been proved to be a method sensitive enough to detect unstructured-to-structured transitions of MeV N_{TAIL} upon binding to P_{XD} (6, 44, 46). Using the same approach, we showed that both NiV and HeV N_{TAIL} undergo α-helical induced folding upon binding to the corresponding P X domain. Binding of *Henipavirus* N_{TAIL} domains to P_{XD} results in the same type of structural transitions as observed with the MeV N_{TAIL}-P_{XD} couple (6, 44, 46) and is in agreement with the strong α-helical propensity of *Henipavirus* N_{TAIL} (14). Note however that these studies remain qualitative; if the estimated α-helical content is useful for comparative purposes, deconvolution approaches notoriously lead to estimations that cannot be taken as fully reliable, *i.e.* they often significantly deviate from the actual content in secondary structure as observed in the experimentally determined structures (for examples see Refs. 44, 117).

The NMR titration experiments of *Henipavirus* N_{TAIL} with increasing amounts of P_{XD} confirmed that a complex is formed between the two partners. For both NiV and HeV, around 15 peaks disappeared from the N_{TAIL} spectrum upon the addition of P_{XD}, whereas only very few peaks underwent chemical shift changes. These observations point toward the intermediate exchange regime often observed for IDPs undergoing folding-upon-binding events (for examples see Refs. 39, 54, 83, and 118). Indeed, although IDPs give rise to sharp NMR resonances because of fast internal motions and short effective correlation times, interactions of disordered regions with folded proteins lead to resonance line broadening of interacting residues because of a larger effective correlation time, restricted local motion, and possible exchange between free and bound states on millisecond to microsecond time scales. Interestingly, in the case of the Hendra couple, no new peaks appeared in the N_{TAIL} spectrum even with saturating amounts of P_{XD}, *i.e.* under conditions in which the fraction of bound N_{TAIL}, as inferred from the measured K_D, was 100%. This behavior, which is in contrast to that observed with the NiV and MeV couple (54), suggests that even when bound to P_{XD}, HeV N_{TAIL} remains dynamic, undergoing exchange between different conformers on the P_{XD} surface. The vanishing of resonances within IDPs upon the addition of a partner protein without the reappearance of the signals at saturation is frequently observed (for examples see (Refs. 119–121). Definite answers about the N_{TAIL} residues that are involved in the interaction with P_{XD} would require the assignment of the NMR spectrum of the free and bound forms, a work that is currently in progress and will be addressed in future studies.

Despite the α-helical transition that both NiV and HeV N_{TAIL} undergo upon binding to P_{XD}, the experimentally determined R_S of the NiV N_{TAIL}-P_{XD} complex suggests that binding to P_{XD} does not imply formation of a compact complex, with this latter rather retaining a considerable flexibility. In further support of this observation, the many observable and relatively sharp NMR resonances in both NiV and HeV N_{TAIL}-P_{XD} complexes, displaying chemical shifts that are nearly unaltered, provide evidence that N_{TAIL} remains significantly disordered even in the bound form. Therefore the final complex is likely endowed with flexible appendages in a structural arrangement possibly reminiscent of that observed in the case of the MeV complex (44) and also proposed for SeV (84).

Structural Models of Henipavirus N_{TAIL}-P_{XD} Complexes and Functional Implications for Transcription and Replication—By analogy with the related MeV (44, 74) and also based on ITC studies carried out in the presence of 1 M NaCl, which showed that the N_{TAIL}-P_{XD} interaction does not rely on polar contacts, we reasoned that the burying of apolar residues of N_{TAIL} at the P_{XD} surface could be the driving force in the P_{XD}-induced folding of N_{TAIL}. Indeed, although globular proteins contribute most of their hydrophobic residues to the protein core, IDPs expose their few hydrophobic residues to the surface, thereby allowing interaction with binding partners. As a result, IDP interfaces make more hydrophobic contacts (33% for IDPs and 22% for ordered proteins), whereas ordered interfaces make

more polar interactions (122). A notable exception is provided by the SeV N_{TAIL}-P_{XD} complex that mainly relies on polar contacts and is therefore impaired by high salt concentrations (83).

We therefore modeled the more hydrophobic side of the amphipathic α-MoRE of N_{TAIL} at the hydrophobic surface delimited by helices α2 and α3 of P_{XD} (74). We emphasize that the proposed models are only a tentative description of a possible mode of interaction. Precise structural information on the molecular mechanism of the induced folding of N_{TAIL} upon binding to P_{XD} awaits the availability of the crystal structure of at least one of the two N_{TAIL}-P_{XD} complexes. Nevertheless, it is noteworthy that interactions similar to those occurring in our models take place not only in the related MeV complex that was used as template but also in many other protein complexes, as well as within individual proteins. Indeed, a search for homologous proteins using the DALI server (123) resulted in numerous hits (Z-score $>$ 2.0), including a complex between an affibody and protein Z (PDB code 1LP1), IgG-binding proteins A and G (PDB codes 2JWD and 1Q2N), and Ebola virus VP35 (PDB code 3L27). These proteins, although exhibiting no significant sequence identity with our models, possess a similar four-helix bundle arrangement, with nevertheless some differences in the angles between the helices and the loops connecting them, leading to r.m.s.d. values ranging from 1.0 to 3.5 Å. The broad occurrence of this type of structural arrangement reflects the fact that the triple helical bundle is a very common structural motif used as a recognition scaffold (124).

Search of the Protein Data Bank database for complexes exhibiting interfaces similar to those of the NiV and HeV complex using the PISA server led to the retrieval of two protein complexes (PDB codes 2IZX and 2D2C, respectively) exhibiting an interface area of 384 and 445 Å^2. The rather small buried interface area of the NiV and HeV complexes (439 and 337 Å^2, respectively) is in agreement with previous reports indicating that the interfaces of complexes involving IDPs are generally smaller than those occurring in ordered complexes (42).

The surface buried in P_{XD} by the α-helix of N_{TAIL} in both *Henipavirus* complexes is smaller than that observed in the MeV complex (634 Å^2), suggesting a less stable complex. That a relationship exists between interface buried surface area and complex stability is commonly accepted and has been clearly established by a recent survey of subunit interfaces of weakly associated protein-protein complexes. Those studies reveal that weak complexes (*e.g.* K_D in the μM range) have loosely packed interfaces that are smaller (by a factor of 2.4 on average) than in tight complexes (125).

The lower buried surface area of the *Henipavirus* N_{TAIL}-P_{XD} complex is consistent with the lower affinity of the binding reaction as compared with the MeV N_{TAIL}-P_{XD} couple. In this latter case, indeed, our previous SPR and fluorescence spectroscopy studies indicated a K_D in the 100 nM range (46), contrary to ITC and SPR studies carried out by Kingston and colleagues (98, 126) that revealed a K_D of 7.4–13 μM. It should be noted however that these latter studies were carried out using N_{TAIL} peptides encompassing residues 477–505 or 477–525 rather than full-length N_{TAIL} (98, 126).

In further support of a less tightly bound complex in henipaviruses, the addition of P_{XD} has no notable impact on the chemical environment of Trp-527 of both NiV and HeV N_{TAIL}, contrary to what was observed in the case of MeV N_{TAIL} where the addition of P_{XD} led to a dose-dependent impact on the fluorescence intensity of Trp-518 (the counterpart of Trp-527) (46). This observation is consistent with a higher conformational flexibility of the C-terminal region of the *Henipavirus* N_{TAIL} domains in the bound form as compared with MeV N_{TAIL}.

Considering that the contact between P_{XD} and N_{TAIL} within the replicative complex has to be dynamically made/broken to allow the polymerase to progress along the nucleocapsid template during both transcription and replication, as well as to deliver N monomers to the nascent RNA chain, the N_{TAIL}-P_{XD} complex cannot be excessively stable for this transition to occur efficiently at a high rate. A relatively labile complex can result either from a tight complex the strength of which is modulated by co-factors or from an inherently lower affinity of the binding reaction. MeV would provide an example of the first scenario, where the high affinity N_{TAIL}-P_{XD} complex is modulated by the major inducible heat shock protein (Hsp70), which acts by destabilizing the complex, thereby promoting cycles of binding and release of the polymerase complex that lead to increased transcription and replication (127–130). A similar high affinity complex has also been observed in the case of rabies virus, where the K_D between N-RNA rings and the C-terminal domain of the phosphoprotein was found to be 160 nM (107). In this latter case, a mechanism different from cartwheeling has been evoked, however, whereby the P protein would be permanently bound to the nucleocapsid template, and the polymerase would jump between adjacent P dimers (see Ref. 131 and references cited therein). On the other hand, SeV (83) and *Henipavirus* would provide examples of the second scenario, with K_D values in the μM range. These findings would support a cartwheeling mechanism for the polymerase complex of *Henipavirus*, as already proposed for other *Paramyxoviridae* members (132, 133). Whatever the mechanism by which the polymerase moves along the template, the present studies, by revealing that P is recruited onto the nucleocapsid template via the N_{TAIL}-P_{XD} interaction, designate this latter as a promising target for antiviral therapies. The relevance of the N_{TAIL}-P_{XD} complex as a target for antiviral drugs is further underscored by recent reports showing that protein-protein interactions mediated by disordered regions are valuable drug discovery targets with the potential to increase significantly the discovery rate for new compounds (see Refs. 134–136 and references cited therein).

Acknowledgments—We thank Christophe Flaudrops, Philippe Decloquement, and the mass spectrometry platform of the IFR48 of Marseille for mass spectrometry analyses. We also thank Gerlind Sulzenbacher (Laboratoire d'Architecture et Fonction des Macromolécules Biologiques) for help with structural modeling and David Veesler for advice on the SEC-MALLS experiments. We thank Frédéric Carrière (Laboratoire d'Enzymologie Interfaciale et de Physiologie de la Lipolyse, Marseille) for useful comments on Fig. 2, 7, and 8.

REFERENCES

1. Eaton, B. T., Mackenzie, J. S., and Wang, L. F. (2007) in *Fields Virology* (Fields, B. N., Knipe, D. M., and Howley, P. M., eds) 5th Ed., pp. 1587–1600, Lippincott-Raven, Philadelphia

2. Wang, L. F., Yu, M., Hansson, E., Pritchard, L. I., Shiell, B., Michalski, W. P., and Eaton, B. T. (2000) *J. Virol.* **74,** 9972–9979
3. Drexler, J. F., Corman, V. M., Gloza-Rausch, F., Seebens, A., Annan, A., Ipsen, A., Kruppa, T., Müller, M. A., Kalko, E. K., Adu-Sarkodie, Y., Oppong, S., and Drosten, C. (2009) *PLoS ONE* **4,** e6367
4. Eaton, B. T., Broder, C. C., Middleton, D., and Wang, L. F. (2006) *Nat. Rev. Microbiol.* **4,** 23–35
5. Karlin, D., Longhi, S., and Canard, B. (2002) *Virology* **302,** 420–432
6. Longhi, S., Receveur-Bréchot, V., Karlin, D., Johansson, K., Darbon, H., Bhella, D., Yeo, R., Finet, S., and Canard, B. (2003) *J. Biol. Chem.* **278,** 18638–18648
7. Schoehn, G., Mavrakis, M., Albertini, A., Wade, R., Hoenger, A., and Ruigrok, R. W. (2004) *J. Mol. Biol.* **339,** 301–312
8. Bhella, D. (2007) in *Measles Virus Nucleoprotein* (Longhi, S., ed) pp. 37–51, Nova Publishers Inc., Hauppage, NY
9. Bhella, D., Ralph, A., Murphy, L. B., and Yeo, R. P. (2002) *J. Gen. Virol.* **83,** 1831–1839
10. Bhella, D., Ralph, A., and Yeo, R. P. (2004) *J. Mol. Biol.* **340,** 319–331
11. Halpin, K., Bankamp, B., Harcourt, B. H., Bellini, W. J., and Rota, P. A. (2004) *J. Gen. Virol.* **85,** 701–707
12. Chan, Y. P., Koh, C. L., Lam, S. K., and Wang, L. F. (2004) *J. Gen. Virol.* **85,** 1675–1684
13. Omi-Furutani, M., Yoneda, M., Fujita, K., Ikeda, F., and Kai, C. (2010) *J. Virol.* **84,** 9793–9799
14. Habchi, J., Mamelli, L., Darbon, H., and Longhi, S. (2010) *PLoS ONE* **5,** e11684
15. Lou, Z., Xu, Y., Xiang, K., Su, N., Qin, L., Li, X., Gao, G. F., Bartlam, M., and Rao, Z. (2006) *FEBS J.* **273,** 4538–4547
16. Bowden, T. A., Crispin, M., Harvey, D. J., Aricescu, A. R., Grimes, J. M., Jones, E. Y., and Stuart, D. I. (2008) *J. Virol.* **82,** 11628–11636
17. Bowden, T. A., Aricescu, A. R., Gilbert, R. J., Grimes, J. M., Jones, E. Y., and Stuart, D. I. (2008) *Nat. Struct. Mol. Biol.* **15,** 567–572
18. Bowden, T. A., Crispin, M., Harvey, D. J., Jones, E. Y., and Stuart, D. I. (2010) *J. Virol.* **84,** 6208–6217
19. Dunker, A. K., Lawson, J. D., Brown, C. J., Williams, R. M., Romero, P., Oh, J. S., Oldfield, C. J., Campen, A. M., Ratliff, C. M., Hipps, K. W., Ausio, J., Nissen, M. S., Reeves, R., Kang, C., Kissinger, C. R., Bailey, R. W., Griswold, M. D., Chiu, W., Garner, E. C., and Obradovic, Z. (2001) *J. Mol. Graph. Model.* **19,** 26–59
20. Dunker, A. K., and Obradovic, Z. (2001) *Nat. Biotechnol.* **19,** 805–806
21. Uversky, V. N. (2002) *Protein Sci.* **11,** 739–756
22. Uversky, V. N. (2003) *Cell. Mol. Life Sci.* **60,** 1852–1871
23. Dyson, H. J., and Wright, P. E. (2005) *Nat. Rev. Mol. Cell Biol.* **6,** 197–208
24. Radivojac, P., Iakoucheva, L. M., Oldfield, C. J., Obradovic, Z., Uversky, V. N., and Dunker, A. K. (2007) *Biophys. J.* **92,** 1439–1456
25. Wright, P. E., and Dyson, H. J. (1999) *J. Mol. Biol.* **293,** 321–331
26. Dunker, A. K., Oldfield, C. J., Meng, J., Romero, P., Yang, J. Y., Chen, J. W., Vacic, V., Obradovic, Z., and Uversky, V. N. (2008) *BMC Genomics* **9,** Suppl. 2, S1
27. Dunker, A. K., Silman, I., Uversky, V. N., and Sussman, J. L. (2008) *Curr. Opin. Struct. Biol.* **18,** 756–764
28. Uversky, V. N. (2010) *J. Biomed. Biotechnol. 2010,* 568068
29. Uversky, V. N., and Dunker, A. K. (2010) *Biochim. Biophys. Acta* **1804,** 1231–1264
30. Turoverov, K. K., Kuznetsova, I. M., and Uversky, V. N. (2010) *Prog. Biophys. Mol. Biol.* **102,** 73–84
31. Jha, A. K., Colubri, A., Freed, K. F., and Sosnick, T. R. (2005) *Proc. Natl. Acad. Sci. U.S.A.* **102,** 13099–13104
32. Bernadó, P., Blanchard, L., Timmins, P., Marion, D., Ruigrok, R. W., and Blackledge, M. (2005) *Proc. Natl. Acad. Sci. U.S.A.* **102,** 17002–17007
33. Kriwacki, R. W., Hengst, L., Tennant, L., Reed, S. I., and Wright, P. E. (1996) *Proc. Natl. Acad. Sci. U.S.A.* **93,** 11504–11509
34. Uversky, V. N. (2002) *Eur. J. Biochem.* **269,** 2–12
35. Dyson, H. J., and Wright, P. E. (2002) *Curr. Opin. Struct. Biol.* **12,** 54–60
36. Fuxreiter, M., Simon, I., Friedrich, P., and Tompa, P. (2004) *J. Mol. Biol.* **338,** 1015–1026
37. Uversky, V. N., Oldfield, C. J., and Dunker, A. K. (2005) *J. Mol. Recognit.* **18,** 343–384
38. Dunker, A. K., Cortese, M. S., Romero, P., Iakoucheva, L. M., and Uversky, V. N. (2005) *FEBS J.* **272,** 5129–5148
39. Sugase, K., Dyson, H. J., and Wright, P. E. (2007) *Nature* **447,** 1021–1025
40. Oldfield, C. J., Cheng, Y., Cortese, M. S., Romero, P., Uversky, V. N., and Dunker, A. K. (2005) *Biochemistry* **44,** 12454–12470
41. Mohan, A., Oldfield, C. J., Radivojac, P., Vacic, V., Cortese, M. S., Dunker, A. K., and Uversky, V. N. (2006) *J. Mol. Biol.* **362,** 1043–1059
42. Vacic, V., Oldfield, C. J., Mohan, A., Radivojac, P., Cortese, M. S., Uversky, V. N., and Dunker, A. K. (2007) *J. Proteome Res.* **6,** 2351–2366
43. Fuxreiter, M., Tompa, P., and Simon, I. (2007) *Bioinformatics* **23,** 950–956
44. Johansson, K., Bourhis, J. M., Campanacci, V., Cambillau, C., Canard, B., and Longhi, S. (2003) *J. Biol. Chem.* **278,** 44567–44573
45. Bourhis, J. M., Johansson, K., Receveur-Bréchot, V., Oldfield, C. J., Dunker, K. A., Canard, B., and Longhi, S. (2004) *Virus Res.* **99,** 157–167
46. Bourhis, J. M., Receveur-Bréchot, V., Oglesbee, M., Zhang, X., Buccellato, M., Darbon, H., Canard, B., Finet, S., and Longhi, S. (2005) *Protein Sci.* **14,** 1975–1992
47. Bourhis, J. M., Canard, B., and Longhi, S. (2005) *Virologie* **9,** 367–383
48. Bourhis, J. M., Canard, B., and Longhi, S. (2006) *Virology* **344,** 94–110
49. Morin, B., Bourhis, J. M., Belle, V., Woudstra, M., Carrière, F., Guigliarelli, B., Fournel, A., and Longhi, S. (2006) *J. Phys. Chem. B* **110,** 20596–20608
50. Bourhis, J. M., and Longhi, S. (2007) in *Measles Virus Nucleoprotein* (Longhi, S., ed) pp. 1–35, Nova Publishers Inc., Hauppage, NY
51. Belle, V., Rouger, S., Costanzo, S., Liquiere, E., Strancar, J., Guigliarelli, B., Fournel, A., and Longhi, S. (2008) *Proteins Struct. Funct. Bioinformat.* **73,** 973–988
52. Longhi, S. (2009) *Curr. Top. Microbiol. Immunol.* **329,** 103–128
53. Bernard, C., Gely, S., Bourhis, J. M., Morelli, X., Longhi, S., and Darbon, H. (2009) *FEBS Lett.* **583,** 1084–1089
54. Gely, S., Lowry, D. F., Bernard, C., Jensen, M. R., Blackledge, M., Costanzo, S., Bourhis, J. M., Darbon, H., Daughdrill, G., and Longhi, S. (2010) *J. Mol. Recognit.* **23,** 435–447
55. Bischak, C. G., Longhi, S., Snead, D. M., Costanzo, S., Terrer, E., and Londergan, C. H. (2010) *Biophys. J.* **99,** 1676–1683
56. Xu, B., Jahic, M., and Enfors, S. O. (1999) *Biotechnol. Prog.* **15,** 81–90
57. Uversky, V. N. (1993) *Biochemistry* **32,** 13288–13298
58. Sambrook, J., Fritsch, E. F., and Maniatis, T. (1989) *Molecular Cloning: A Laboratoty Manual*, 2nd Ed., Cold Spring Harbor Laboratory Press, New York
59. Whitmore, L., and Wallace, B. A. (2004) *Nucleic Acids Res.* **32,** W668–W673
60. Whitmore, L., and Wallace, B. A. (2008) *Biopolymers* **89,** 392–400
61. Hwang, T. L., and Shaka, A. J. (1998) *J. Magn. Reson.* **135,** 280–287
62. Delaglio, F., Grzesiek, S., Vuister, G. W., Zhu, G., Pfeifer, J., and Bax, A. (1995) *J. Biomol. NMR* **6,** 277–293
63. Vranken, W. F., Boucher, W., Stevens, T. J., Fogh, R. H., Pajon, A., Llinas, M., Ulrich, E. L., Markley, J. L., Ionides, J., and Laue, E. D. (2005) *Proteins* **59,** 687–696
64. Schuck, P. (1997) *Annu. Rev. Biophys. Biomol. Struct.* **26,** 541–566
65. Kalinin, N. L., Ward, L. D., and Winzor, D. J. (1995) *Anal. Biochem.* **228,** 238–244
66. Ferron, F., Rancurel, C., Longhi, S., Cambillau, C., Henrissat, B., and Canard, B. (2005) *J. Gen. Virol.* **86,** 743–749
67. Larkin, M. A., Blackshields, G., Brown, N. P., Chenna, R., McGettigan, P. A., McWilliam, H., Valentin, F., Wallace, I. M., Wilm, A., Lopez, R., Thompson, J. D., Gibson, T. J., and Higgins, D. G. (2007) *Bioinformatics* **23,** 2947–2948
68. Gouet, P., Courcelle, E., Stuart, D. I., and Métoz, F. (1999) *Bioinformatics* **15,** 305–308
69. Bryson, K., McGuffin, L. J., Marsden, R. L., Ward, J. J., Sodhi, J. S., and Jones, D. T. (2005) *Nucleic Acids Res.* **33,** W36–38
70. Karplus, K., Karchin, R., Draper, J., Casper, J., Mandel-Gutfreund, Y., Diekhans, M., and Hughey, R. (2003) *Proteins* **53,** Suppl. 6, 491–496
71. Karchin, R., Cline, M., Mandel-Gutfreund, Y., and Karplus, K. (2003)

Proteins **51,** 504–514
72. Karplus, K., Katzman, S., Shackleford, G., Koeva, M., Draper, J., Barnes, B., Soriano, M., and Hughey, R. (2005) *Proteins* **61,** Suppl. 7, 135–142
73. Guex, N., and Peitsch, M. C. (1997) *Electrophoresis* **18,** 2714–2723
74. Kingston, R. L., Hamel, D. J., Gay, L. S., Dahlquist, F. W., and Matthews, B. W. (2004) *Proc. Natl. Acad. Sci. U.S.A.* **101,** 8301–8306
75. van Gunsteren, W. F., Billeter, S. R., Eising, A. A., Hünenberger, P. H., Krüger, P., Mark, A. E., Scott, W. R. P., and Tironi, I. G. (1996) *Biomolecular Simulation: the GROMOS96 Manual and User Guide*, vdf Hochschuverlag, Zürich
76. Emsley, P., and Cowtan, K. (2004) *Acta Crystallogr. D Biol. Crystallogr.* **60,** 2126–2132
77. Davis, I. W., Leaver-Fay, A., Chen, V. B., Block, J. N., Kapral, G. J., Wang, X., Murray, L. W., Arendall, W. B., 3rd, Snoeyink, J., Richardson, J. S., and Richardson, D. C. (2007) *Nucleic Acids Res.* **35,** W375–383
78. Krissinel, E., and Henrick, K. (2007) *J. Mol. Biol.* **372,** 774–797
79. DeLano, W. L. (2002) *Proteins Struct. Funct. Bioinformat.* **30,** 442–454
80. Kerdiles, Y. M., Cherif, B., Marie, J. C., Tremillon, N., Blanquier, B., Libeau, G., Diallo, A., Wild, T. F., Villiers, M. B., and Horvat, B. (2006) *Viral Immunol.* **19,** 324–334
81. Frottin, F., Martinez, A., Peynot, P., Mitra, S., Holz, R. C., Giglione, C., and Meinnel, T. (2006) *Mol. Cell. Proteomics* **5,** 2336–2349
82. Freyer, M. W., and Lewis, E. A. (2008) *Methods Cell Biol.* **84,** 79–113
83. Houben, K., Marion, D., Tarbouriech, N., Ruigrok, R. W., and Blanchard, L. (2007) *J. Virol.* **81,** 6807–6816
84. Jensen, M. R., Houben, K., Lescop, E., Blanchard, L., Ruigrok, R. W., and Blackledge, M. (2008) *J. Am. Chem. Soc.* **130,** 8055–8061
85. Karlin, D., Longhi, S., Receveur, V., and Canard, B. (2002) *Virology* **296,** 251–262
86. Tompa, P. (2002) *Trends Biochem. Sci.* **27,** 527–533
87. Tell, G., Perrone, L., Fabbro, D., Pellizzari, L., Pucillo, C., De Felice, M., Acquaviva, R., Formisano, S., and Damante, G. (1998) *Biochem. J.* **329,** 395–403
88. Hua, Q. X., Jia, W. H., Bullock, B. P., Habener, J. F., and Weiss, M. A. (1998) *Biochemistry* **37,** 5858–5866
89. Dahlman-Wright, K., and McEwan, I. J. (1996) *Biochemistry* **35,** 1323–1327
90. Berman, H. M., Westbrook, J., Feng, Z., Gilliland, G., Bhat, T. N., Weissig, H., Shindyalov, I. N., and Bourne, P. E. (2000) *Nucleic Acids Res.* **28,** 235–242
91. Lambert, C., Léonard, N., De Bolle, X., and Depiereux, E. (2002) *Bioinformatics* **18,** 1250–1256
92. Arnold, K., Bordoli, L., Kopp, J., and Schwede, T. (2006) *Bioinformatics* **22,** 195–201
93. Fontana, A., Polverino de Laureto, P., De Filippis, V., Scaramella, E., and Zambonin, M. (1997) *Fold. Des.* **2,** R17–R26
94. Fontana, A., Zambonin, M., De Filippis, V., Bosco, M., and Polverino de Laureto, P. (1995) *FEBS Lett.* **362,** 266–270
95. Fontana, A., Polverino de Laureto, P., Spolaore, B., Frare, E., and Zambonin, M. (2010) *Instrumental Analysis of Intrinsically Disordered Proteins: Assessing Structure and Conformation* (Uversky, V., and Longhi, S. eds) pp. 569–626, John Wiley and Sons, Hoboken, NJ
96. Receveur-Bréchot, V., Bourhis, J. M., Uversky, V. N., Canard, B., and Longhi, S. (2006) *Proteins Struct. Funct. Bioinformat.* **62,** 24–45
97. Kingston, R. L., Gay, L. S., Baase, W. S., and Matthews, B. W. (2008) *J. Mol. Biol.* **379,** 719–731
98. Kingston, R. L., Walter, A. B., and Gay, L. S. (2004) *J. Virol.* **78,** 8630–8640
99. Tarbouriech, N., Curran, J., Ebel, C., Ruigrok, R. W., and Burmeister, W. P. (2000) *Virology* **266,** 99–109
100. Tarbouriech, N., Curran, J., Ruigrok, R. W., and Burmeister, W. P. (2000) *Nat. Struct. Biol.* **7,** 777–781
101. Marion, D., Tarbouriech, N., Ruigrok, R. W., Burmeister, W. P., and Blanchard, L. (2001) *J. Biomol. NMR* **21,** 75–76
102. Blanchard, L., Tarbouriech, N., Blackledge, M., Timmins, P., Burmeister, W. P., Ruigrok, R. W., and Marion, D. (2004) *Virology* **319,** 201–211
103. Assenberg, R., Delmas, O., Morin, B., Graham, S. C., De Lamballerie, X., Laubert, C., Coutard, B., Grimes, J. M., Neyts, J., Owens, R. J., Brandt, B. W., Gorbalenya, A., Tucker, P., Stuart, D. I., Canard, B., and Bourhy, H. (2010) *Antiviral Res.* **87,** 149–161
104. Gerard, F. C., Ribeiro Ede, A., Jr., Leyrat, C., Ivanov, I., Blondel, D., Longhi, S., Ruigrok, R. W., and Jamin, M. (2009) *J. Mol. Biol.* **388,** 978–996
105. Ivanov, I., Crépin, T., Jamin, M., and Ruigrok, R. W. (2010) *J. Virol.* **84,** 3707–3710
106. Ribeiro, E. A., Jr., Favier, A., Gerard, F. C., Leyrat, C., Brutscher, B., Blondel, D., Ruigrok, R. W., Blackledge, M., and Jamin, M. (2008) *J. Mol. Biol.* **382,** 525–538
107. Ribeiro, E. D., Jr., Leyrat, C., Gerard, F. C., Albertini, A. A., Falk, C., Ruigrok, R. W., and Jamin, M. (2009) *J. Mol. Biol.*
108. Fogg, M. J., Alzari, P., Bahar, M., Bertini, I., Betton, J. M., Burmeister, W. P., Cambillau, C., Canard, B., Corrondo, M. A., Coll, M., Daenke, S., Dym, O., Egloff, M. P., Enguita, F. J., Geerlof, A., Haouz, A., Jones, T. A., Ma, Q., Manicka, S. N., Migliardi, M., Nordlund, P., Owens, R. J., Peleg, Y., Schneider, G., Schnell, R., Stuart, D. I., Tarbouriech, N., Unge, T., Wilkinson, A. J., Wilmanns, M., Wilson, K. S., Zimhony, O., and Grimes, J. M. (2006) *Acta Crystallogr. D Biol. Crystallogr.* **62,** 1196–1207
109. Albeck, S., Alzari, P., Andreini, C., Banci, L., Berry, I. M., Bertini, I., Cambillau, C., Canard, B., Carter, L., Cohen, S. X., Diprose, J. M., Dym, O., Esnouf, R. M., Felder, C., Ferron, F., Guillemot, F., Hamer, R., Ben Jelloul, M., Laskowski, R. A., Laurent, T., Longhi, S., Lopez, R., Luchinat, C., Malet, H., Mochel, T., Morris, R. J., Moulinier, L., Oinn, T., Pajon, A., Peleg, Y., Perrakis, A., Poch, O., Prilusky, J., Rachedi, A., Ripp, R., Rosato, A., Silman, I., Stuart, D. I., Sussman, J. L., Thierry, J. C., Thompson, J. D., Thornton, J. M., Unger, T., Vaughan, B., Vranken, W., Watson, J. D., Whamond, G., and Henrick, K. (2006) *Acta Crystallogr. D Biol. Crystallogr.* **62,** 1184–1195
110. Mastrangelo, E., Milani, M., Bollati, M., Selisko, B., Peyrane, F., Pandini, V., Sorrentino, G., Canard, B., Konarev, P. V., Svergun, D. I., de Lamballerie, X., Coutard, B., Khromykh, A. A., and Bolognesi, M. (2007) *J. Mol. Biol.* **372,** 444–455
111. Malet, H., Egloff, M. P., Selisko, B., Butcher, R. E., Wright, P. J., Roberts, M., Gruez, A., Sulzenbacher, G., Vonrhein, C., Bricogne, G., Mackenzie, J. M., Khromykh, A. A., Davidson, A. D., and Canard, B. (2007) *J. Biol. Chem.* **282,** 10678–10689
112. Canard, B., Joseph, J. S., and Kuhn, P. (2008) *Antiviral Res.* **78,** 47–50
113. Malet, H., Coutard, B., Jamal, S., Dutartre, H., Papageorgiou, N., Neuvonen, M., Ahola, T., Forrester, N., Gould, E. A., Lafitte, D., Ferron, F., Lescar, J., Gorbalenya, A. E., de Lamballerie, X., and Canard, B. (2009) *J. Virol.* **83,** 6534–6545
114. Morin, B., Coutard, B., Lelke, M., Ferron, F., Kerber, R., Jamal, S., Frangeul, A., Baronti, C., Charrel, R., de Lamballerie, X., Vonrhein, C., Lescar, J., Bricogne, G., Gunther, S., and Canard, B. (2010) *PLoS Pathog. 2010* **6,** e1001038
115. Coutard, B., and Canard, B. (2010) *Antiviral Res.* **87,** 85–94
116. Gorbalenya, A. E., Lieutaud, P., Harris, M. R., Coutard, B., Canard, B., Kleywegt, G. J., Kravchenko, A. A., Samborskiy, D. V., Sidorov, I. A., Leontovich, A. M., and Jones, T. A. (2010) *Antiviral Res.* **87,** 95–110
117. Couturier, M., Buccellato, M., Costanzo, S., Bourhis, J. M., Shu, Y., Nicaise, M., Desmadril, M., Flaudrops, C., Longhi, S., and Oglesbee, M. (2010) *J. Mol. Recognit.* **23,** 301–315
118. Ferreon, J. C., Martinez-Yamout, M. A., Dyson, H. J., and Wright, P. E. (2009) *Proc. Natl. Acad. Sci. U.S.A.* **106,** 13260–13265
119. Mittag, T., Orlicky, S., Choy, W. Y., Tang, X., Lin, H., Sicheri, F., Kay, L. E., Tyers, M., and Forman-Kay, J. D. (2008) *Proc. Natl. Acad. Sci. U.S.A.* **105,** 17772–17777
120. Sue, S. C., Cervantes, C., Komives, E. A., and Dyson, H. J. (2008) *J. Mol. Biol.* **380,** 917–931
121. Kiss, R., Bozoky, Z., Kovács, D., Róna, G., Friedrich, P., Dvortsák, P., Weisemann, R., Tompa, P., and Perczel, A. (2008) *FEBS Lett.* **582,** 2149–2154
122. Mészáros, B., Tompa, P., Simon, I., and Dosztányi, Z. (2007) *J. Mol. Biol.* **372,** 549–561
123. Holm, L., and Sander, C. (1993) *J. Mol. Biol.* **233,** 123–138
124. Hosse, R. J., Rothe, A., and Power, B. E. (2006) *Protein Sci.* **15,** 14–27

125. Dey, S., Pal, A., Chakrabarti, P., and Janin, J. (2010) *J. Mol. Biol.* **398,** 146–160
126. Yegambaram, K., and Kingston, R. L. (2010) *Protein Sci.* **19,** 893–899
127. Zhang, X., Glendening, C., Linke, H., Parks, C. L., Brooks, C., Udem, S. A., and Oglesbee, M. (2002) *J. Virol.* **76,** 8737–8746
128. Zhang, X., Bourhis, J. M., Longhi, S., Carsillo, T., Buccellato, M., Morin, B., Canard, B., and Oglesbee, M. (2005) *Virology* **337,** 162–174
129. Carsillo, T., Zhang, X., Vasconcelos, D., Niewiesk, S., and Oglesbee, M. (2006) *J. Virol.* **80,** 2904–2912
130. Oglesbee, M. (2007) in *Measles Virus Nucleoprotein* (Longhi, S., ed) pp. 53–98, Nova Publishers Inc., Hauppage, NY
131. Leyrat, C., Gérard, F. C., de Almeida Ribeiro, E., Jr., Ivanov, I., Ruigrok, R. W., and Jamin, M. (2010) *Protein Pept. Lett.* **17,** 979–987
132. Curran, J., and Kolakofsky, D. (1999) *Adv. Virus Res.* **54,** 403–422
133. Kolakofsky, D., Le Mercier, P., Iseni, F., and Garcin, D. (2004) *Virology* **318,** 463–473
134. Cheng, Y., LeGall, T., Oldfield, C. J., Mueller, J. P., Van, Y. Y., Romero, P., Cortese, M. S., Uversky, V. N., and Dunker, A. K. (2006) *Trends Biotechnol.* **24,** 435–442
135. Uversky, V. N. (2010) *Expert Rev. Proteomics* **7,** 543–564
136. Dunker, A. K., and Uversky, V. N. (2010) *Curr. Opin. Pharmacol.* **10,** 782–788